

Complexity of quantum trajectories

Luca Lumia ,^{1,2} Emanuele Tirrito,^{3,4} Mario Collura ,^{1,5} Fabian H.L. Essler,⁶ and Rosario Fazio ^{3,4}

¹*SISSA, via Bonomea 265, 34136 Trieste, Italy*

²*University of Strasbourg and CNRS, CESQ and ISIS, 67000 Strasbourg, France*

³*The Abdus Salam International Center for Theoretical Physics, Strada Costiera 11, 34151 Trieste, Italy*

⁴*Dipartimento di Fisica “E. Pancini”, Università di Napoli “Federico II”, Monte S. Angelo, I-80126 Napoli, Italy*

⁵*INFN, Sezione di Trieste, Via Valerio 2, 34127 Trieste, Italy*

⁶*The Rudolf Peierls Centre for Theoretical Physics, Oxford University, Oxford OX1 3PU, UK*

(Dated: February 3, 2026)

Open quantum systems can be described by unraveling Lindblad master equations into ensembles of quantum trajectories. Here we investigate how the complexity of such trajectories is affected by conservation laws and other dynamical constraints of the underlying Lindblad evolution. We characterize this complexity using a data-driven approach based on the intrinsic dimension, defined as the minimal number of variables required to encode the information contained in a data set. Applying this framework to several systems, including variants of the quantum top and of the XXZ chain, we find that the intrinsic dimension is sensitive to the structure of their dynamics. The Lindblad evolution in these systems is typically chaotic, but additional constraints arise at specific parameter values, where the dynamics becomes integrable, exhibits Hilbert-space fragmentation, or develops a closed BBGKY hierarchy, leading to pronounced minima in the intrinsic dimension. Our approach results in an unsupervised probe of the complexity of dissipative quantum systems that is sensitive to chaos and ergodicity breaking phenomena beyond the initial transient regime.

I. INTRODUCTION

Understanding and quantifying the complexity of quantum many-body dynamics is essential for several reasons. At a fundamental level, complexity governs the spreading of information and the onset of thermalization in closed quantum systems, shaping our understanding of irreversibility and emergent statistical mechanics. Furthermore, complexity determines the extent of classical simulability. Several quantities have been introduced to characterize its many distinct facets. Quantum resources, such as entanglement, non-stabilizerness, and non-Gaussianity, are measures of the computational complexity of the underlying dynamics [1–7]. Krylov complexity and Nielsen’s geometric complexity, capture the scrambling of quantum information, i.e. how deeply the system explores its Hilbert space, with interesting connections to gravitational properties in the context of holographic dualities [8–13].

These quantifiers suggest that ergodic systems are typically complex, displaying strong information scrambling and rapid growth of the associated quantum resources [14–21]. In contrast, ergodicity-breaking systems are governed by the existence of additional constraints on their dynamics. The prototypical example is integrability, which gives rise to an extensive set of conserved quantities with spatially local densities [22, 23]. Other relevant phenomena include localization, which suppresses quantum correlations and leads to slow entanglement growth and frozen operator dynamics [24, 25], quantum many-body scars, which generate atypical trajectories with sub-thermal entanglement within an otherwise ergodic spectrum [26, 27], and Hilbert-space fragmentation, associated to disconnected dynamical sectors and thus may reduce the overall complexity [28, 29].

Originally formulated for unitary dynamics, these concepts have recently been extended to the domain of open quantum systems [30–38]. Recent experimental and theoretical advances have enable the controlled engineering of dissipation channels in synthetic quantum matter and enabled increasingly accurate characterizations of open-system properties through many-body techniques, particularly in systems governed by Lindblad dynamics [39–42]. Integrability in the context of Lindblad equations can be defined by mapping the latter to an imaginary time Schrödinger equation with non-Hermitian Hamiltonian. A number of notable cases have been identified [30, 31, 33, 34, 43–45], including examples exhibiting “operator-space fragmentation” [32, 33, 35, 46]. A mechanism that is a priori separate from integrability and influences the structure of open-system dynamics is the decoupling of the Bogoliubov-Born-Green-Kirkwood-Yvon (BBGKY) hierarchy, which leads to a substantial simplification in the evolution of correlation functions [47]. This property is a particular case of operator space fragmentation and has been exploited to obtain exact results in Lindblad equations that are not necessarily integrable [48–51]. One observable consequence of the BBGKY decoupling is the absence of hydrodynamic tails in the late-time behavior of certain observables due to kinematic reasons [51].

Ergodic and integrable dynamics both give rise to characteristic signatures in the spectrum of the time-evolution operator. For isolated quantum systems, the famous Bohigas-Giannoni-Schmidt and Berry-Tabor conjectures connect the regularity of the dynamics to the spectral statistics of the Hamiltonian: systems with a chaotic semiclassical limit are associated to eigenvalue distributions that follow random matrix theory statistics, while integrable models follow Poisson statistics

[52, 53]. The extension of this correspondence to open quantum maps has become known as the Grobe-Haake-Sommers (GHS) conjecture, suggesting that classically chaotic maps should arise from a Lindbladian whose complex eigenvalues follow the non-Hermitian Ginibre ensembles [54, 55]. The picture turned out to be richer. Indeed, it was later found that dissipative quantum chaos, as characterized by the spectral statistics (i.e. the non-Hermitian Ginibre ensemble), could appear even in the presence of classically regular behavior [56, 57]. In this manuscript, we provide a further example of this phenomenon. The analysis of the spectrum of the Lindbladian was also performed in several different models, without a semiclassical limit [58–60]. For dissipative systems, genuinely quantum dynamical distinctions between chaotic and regular motion have been elusive. This is because the density matrix ultimately relaxes to a steady state determined solely by the dominant eigenvalue of the Lindbladian, which makes it largely insensitive to the detailed structure of the spectrum. While the Grobe–Haake–Sommers (GHS) conjecture identifies chaos through the spectral properties of the Lindbladian, such spectral signatures do not necessarily manifest in the long-time evolution of observables. Consequently, any signatures of dissipative chaos can typically be observed only during the transient dynamics, before the system reaches its steady state [56, 61–64].

In this work we take a different route to characterizing ergodic and non-ergodic behavior in open quantum systems: we take inspiration from classical dynamics, where (non)ergodicity is directly observable in the structure of phase space trajectories, for example through Lyapunov sensitivity or the emergence of fractal attractors in driven-dissipative models [65, 66]. In the quantum setting, this analogy is generally approximate: it can be formalized through semiclassical phase-space representations, which allow one to capture signatures reminiscent of classical chaos. However, these features may be smoothed out or altered by genuine quantum effects, small system sizes, or strong dissipation.

A natural framework for exploring ergodicity in open quantum systems is provided by *quantum trajectories* (QT), which unravel the Lindblad equation into a stochastic process that recovers the density matrix upon averaging [67–69]. By monitoring the quantum system along a single trajectory, the evolution consists of a smooth (non-Hermitian) dynamics, punctuated by stochastic terms dependent on the type of monitoring, that account for interactions with the external environment. When a steady state is reached, the QT do not necessarily become stationary, allowing one to observe dynamical effects beyond the initial transient regime. Our approach is in part motivated by the fact that in certain semiclassical models, it has been observed that QT approach the attractors of the limiting classical system [70, 71], suggesting that individual trajectories can exhibit traces of quantum chaos. Our analysis goes well beyond the semiclassical limit and we will show that the

properties of many-body Lindblad dynamics are reflected in the structure of the associated ensembles of QT.

We quantify the complexity of trajectories in Hilbert space by means of their *intrinsic dimension*. This complexity metric has its mathematical roots in classical information theory and in the theory of fractals. It is a fundamental concept in the field of manifold learning and is commonly used as a preamble to dimensional reduction [72–74]. Machine learning tools have emerged as powerful methods for analyzing complex, high-dimensional data sets, which are an intrinsic property of quantum many-body physics. Their effectiveness relies on the insight that high-dimensionality often arises from the representation of the data set, while correlations can be effectively described by data points embedded on a manifold with few relevant degrees of freedom, which are what the intrinsic dimension quantifies. The connection of intrinsic dimension with information theory is based on Kolmogorov complexity, which sets the theoretical limit on the compressibility of information [75, 76]. This notion represents a facet of complexity that is complementary to computational complexity, which, in a quantum-mechanical context, is more closely related to quantum resources or Nielsen’s complexity. Chaotic classical dynamical systems are known to give rise to a high Kolmogorov complexity. The rate at which this complexity grows can be quantified by the Kolmogorov–Sinai entropy, as established by Brudno’s theorem [77, 78]. Chaotic trajectories often explore higher-dimensional structures known as strange attractors, whose geometry can be characterized by fractal-dimension estimation algorithms that have also been employed to infer the intrinsic dimension of generic datasets [65, 74, 79–82]. The intrinsic dimension also plays an important role as a complexity measure in unsupervised learning applications [81, 83–90]. Related ideas have been successfully applied to statistical mechanics, identifying for instance phase transitions [91–93] or revealing hidden structures in synthetic and experimental data such as snapshots of ultra-cold atoms, outputs of quantum simulators [94] and unitary quantum scars [95]. In our approach, datasets are constructed from ensembles of QT, allowing us to effectively quantify their complexity. We perform a numerical investigation of classes of Lindblad equations exhibiting structurally distinct types of dynamics, with particular attention to the dichotomy between dissipative integrability and chaos, and to the decoupling of correlation functions. Our main result is to show that the intrinsic dimension effectively captures the complexity of the underlying dynamics.

This manuscript is structured as follows. Before embarking on the analysis of particular models we present a summary of our main results in Section II. In Section III we then introduce the Lindblad formalism and discuss spectral properties and the Lindblad analog of the BBGKY hierarchy. This serves as a point of reference for the discussion of our results. In Section IV we define QT and discuss how their complexity can be quan-

tified in terms of their intrinsic dimension. In Sections V and VI we investigate several models that exemplify different mechanisms of ergodicity breaking. Our analysis is based on a specific unraveling, namely quantum jumps. The robustness of our conclusions against alternative unravelings is examined in Section VII. Our main findings are summarized in Section VIII. A discussion of the semi-classical limit of the quantum top and details of our numerical analysis are relegated to appendices.

II. MODEL SELECTION RATIONALE AND SUMMARY OF RESULTS

As mentioned above, our analysis of the complexity of open system dynamics is based on the intrinsic dimension of QT, a data-driven measure that captures the spreading of QT in Hilbert space. We have applied this method to a set of single- and many-body models, corresponding respectively to variants of the quantum top and the spin-1/2 Heisenberg XXZ-spin chain with dissipation. These systems were chosen because they are generically ergodic except for some fine-tuned choices of parameters, each representing a distinct mechanism of ergodicity breaking.

The quantum top is a simple system whose degrees of freedom are defined by the components of a single angular momentum operator S_α , $\alpha = x, y, z$, which we fix in a spin-S representation. We then consider the following time-dependent Hamiltonian

$$\hat{H}(\omega_x, \omega_z, g, k) = \hat{H}_0 + \sum_{n=-\infty}^{\infty} \delta(t - n\tau) \hat{H}_k, \quad (1)$$

where we have defined

$$\hat{H}_0 = \omega_z \hat{S}_z + \frac{g}{S} \hat{S}_z^2 + \omega_x \hat{S}_x, \quad H_k = \frac{k}{S} \hat{S}_y^2. \quad (2)$$

Ladder operators are defined as $\hat{S}_\pm = \hat{S}_x \pm i\hat{S}_y$. We couple the spin to a dissipative environment that polarizes it in the negative- z direction. In Section V we show that the corresponding Lindblad equation features three different regimes: (i) quantum integrable with regular classical limit; (ii) quantum chaotic with chaotic classical limit; and (iii) quantum chaotic with regular orbits in the classical limit.

We then turn to the many-body case and investigate the effects of integrability and of the decoupling of the BBGKY hierarchy on the intrinsic dimension by considering appropriate perturbations of the integrable XXZ model with dephasing introduced in Ref. [30] and of the fragmented model of Ref. [32]. The corresponding Hamiltonian parts are particular cases of

$$\begin{aligned} \hat{H}(J_1, J_2, \Delta) = & \sum_{j=1}^{L-1} J_1 \left[\hat{\sigma}_j^x \hat{\sigma}_{j+1}^x + \hat{\sigma}_j^y \hat{\sigma}_{j+1}^y \right] + \Delta \hat{\sigma}_j^z \hat{\sigma}_{j+1}^z \\ & + J_2 \sum_{j=1}^{L-2} \left(\hat{\sigma}_j^x \hat{\sigma}_{j+1}^x + \hat{\sigma}_j^y \hat{\sigma}_{j+1}^y \right), \end{aligned} \quad (3)$$

Driven-dissipative quantum top with collective damping	
Hamiltonian (autonomous/kicked)	$\hat{H}(\omega_x, \omega_z, g, k)$
Lindblad operator	$\hat{L} = \sqrt{\gamma} \hat{S}_-$
$\omega_x = k = 0$	Quantum and classically integrable
$k \neq 0$	Quantum chaotic, classically chaotic
$\omega_x \neq 0$	Quantum chaotic, classically integrable

TABLE I. A summary of the different parameter regimes of the driven-dissipative quantum top analyzed in Section V. The Hamiltonian is defined in Eq.(1). Depending on the choice of the couplings ω_x, ω_z, k , different dynamical regimes can be explored.

where $\hat{\sigma}_j^\alpha$, $\alpha \in \{x, y, z\}$ denote the Pauli matrices acting on the site $j \in \{1, \dots, N\}$. The various Lindblad operators we consider in Section VI are given in Table II.

Our results can be summarized as follows.

- For the quantum top, the intrinsic dimension of QT discriminates between regular and chaotic regimes: trajectories in integrable settings form effectively one-dimensional manifolds, while chaos, either induced by autonomous or time-dependent perturbations, produces higher-dimensional structures analogous to chaotic attractors. Notably, the intrinsic dimension agrees with the spectral signatures of chaos in the regime with a classical limit, suggesting that the random matrix theory criterion should hold even in absence of the quantum/classical correspondence. As it will be discussed in the forthcoming sections, the quantum top suffers from severe finite size corrections, due to the fact that the different blocks of the Hilbert space grow polynomially with S .
- The spatially extended many-body systems in Table II no longer give rise to one-dimensional QT. However, the intrinsic dimension generally exhibits a sharp minimum at integrable points in parameter space, confirming that integrability structurally suppresses the complexity of QT. In cases where the BBGKY hierarchy decouples, similar reductions are observed. The presence of strong symmetries must be taken carefully into account, since it can also affect the structure of QT through the mechanism of dissipative freezing [96, 97].
- The observations summarized above appear to be independent of the unraveling of the Lindblad equation. More precisely, while the quantitative value

of the intrinsic dimension is unraveling-dependent, we find that its qualitative behavior is robust, with minima consistently identifying regimes with constrained dynamics.

III. LINDBLAD DYNAMICS

The state of an open quantum system is characterized by the density matrix ρ , and under the hypothesis of Markovian dynamics, its time evolution is described by the Lindblad equation [40, 98, 99]

$$\frac{d\hat{\rho}}{dt} = -i[\hat{H}, \hat{\rho}] + \sum_{\alpha} \left(\hat{L}_{\alpha} \hat{\rho} \hat{L}_{\alpha}^{\dagger} - \frac{1}{2} \{ \hat{L}_{\alpha}^{\dagger} \hat{L}_{\alpha}, \hat{\rho} \} \right). \quad (4)$$

Here \hat{H} is the Hamiltonian acting on the system degrees of freedom, while the Lindblad (jump) operators \hat{L}_{α} describe the effect of the environment. They are proportional to $\sqrt{\gamma_{\alpha}}$, where $\gamma_{\alpha} \geq 0$ are the corresponding dissipation rates [40]. The dynamics can be influenced by structural properties such as integrability and the decoupling of correlation functions, that we review below.

A. Dissipative integrability

Let us consider a one-dimensional spin chain with L sites and Hilbert space $\mathcal{H} \cong (\mathbb{C}^2)^{\otimes L}$ that evolves under a local Lindblad equation. It is convenient to employ the standard ‘‘vectorization’’ map $|i\rangle\langle j| \rightarrow |i\rangle|j\rangle$, whose outcome is to represent the density matrix $\hat{\rho} \in \text{End}(\mathcal{H}) \cong \mathcal{H}^* \otimes \mathcal{H}$ as a state vector $|\rho\rangle\rangle \in \mathcal{H} \otimes \mathcal{H}$. In this representation, super-operators are represented by matrices on $\mathcal{H} \otimes \mathcal{H}$, which we denote using a check symbol. The Lindblad equation then takes the form

$$\frac{d}{dt} |\rho\rangle\rangle = \check{\mathcal{L}} |\rho\rangle\rangle \equiv (-i\check{\mathcal{H}} + \check{\mathcal{D}}) |\rho\rangle\rangle, \quad (5)$$

where

$$\begin{aligned} \check{\mathcal{H}} &= \hat{H} \otimes \hat{\mathbb{I}} - \hat{\mathbb{I}} \otimes \hat{H}^*, \\ \check{\mathcal{D}} &= \sum_{\alpha} \left(\hat{L}_{\alpha} \otimes \hat{L}_{\alpha}^* - \frac{1}{2} [\hat{L}_{\alpha}^{\dagger} \hat{L}_{\alpha} \otimes \hat{\mathbb{I}} + \hat{\mathbb{I}} \otimes (\hat{L}_{\alpha}^{\dagger} \hat{L}_{\alpha})^*] \right). \end{aligned}$$

The Lindbladian $\check{\mathcal{L}}$ can then be interpreted as a non-Hermitian Hamiltonian of a system with doubled degrees of freedom, in this case a 2-leg ladder [31], and a sufficient condition for integrability is then that $\check{\mathcal{L}}$ can be obtained from a solution of the Yang-Baxter equation [22]. The Lindblad structure of $\check{\mathcal{L}}$ imposes constraints in addition to integrability, but many examples have been identified in recent years [30–34]. A different mechanism that can significantly constrain Lindbladian dynamics is operator-space fragmentation [32], which is the open quantum system analog of Hilbert-space fragmentation [29]. In fragmented models, there is a large number of subspaces that

are left invariant by the dynamics. In some cases the projections of the Lindbladian onto these ‘‘fragments’’ can be integrable [32, 33].

An important difference between the quantum integrability of Schrödinger and Lindblad equations arises from their symmetries. In integrable models describing unitary time evolution it is possible to construct an extensive set of quasi-local operators that commute with the Hamiltonian and one another. In integrable dissipative models one instead obtains super-operators that commute with the Lindbladian and one another. This condition identifies a *weak symmetry* and is no longer sufficient to define conservation laws: in this context the expectation values of operators are preserved only by *strong symmetries* defined by operators that commute separately with the Hamiltonian and with all Lindblad operators [100, 101].

The distinction between integrable and chaotic behavior is typically reflected in its level-spacing distributions. Having complex eigenvalues, the relevant spacings are the distances $s_j = |\lambda_j - \lambda_j^{nn}|$ between each eigenvalue λ_j and its nearest neighbor λ_j^{nn} in the complex plane, which are distributed according to generalizations of the Poisson/Wigner-Dyson statistics of chaotic/integrable Hamiltonians [54]. For an integrable Lindbladian, s is distributed according to a 2d Poisson process in the complex plane

$$p_P^{(2D)}(s) = \frac{\pi s}{2} e^{-\frac{\pi}{4}s^2}. \quad (6)$$

Even though $p(s) \propto s$, there is no level repulsion in the complex plane because the s is a Jacobian factor. Chaotic Lindbladians instead have spacings distributed like those of the eigenvalues of non-Hermitian random matrices. These are described by the Ginibre ensemble

$$p_{\text{GinUE}}(s) = \prod_{k=1}^{\infty} \frac{\Gamma(1+k, s^2)}{k!} \sum_{j=1}^{\infty} \frac{2s^{2j+1} e^{-s^2}}{\Gamma(1+j, s^2)}, \quad (7)$$

where $\Gamma(1+k, s^2) = \int_{s^2}^{+\infty} t^k e^{-t} dt$ is the incomplete Gamma function. Expanding for $s \rightarrow 0$ results in a $p(s) \sim s^3$ level repulsion, which is independent of the symmetry class for the three Ginibre ensembles GinOE, GinUE, GinSE, unlike for the unitary ensembles GOE, GUE, GSE [54]. In practice, working with a single Lindbladian, the distribution of its eigenvalues is going to be dominated by their density, which is highly model dependent, and it is the distribution of the ‘‘unfolded’’ eigenvalues that should follow the random matrix theory ensembles [102]. Unfolding amounts to removing the effect of the local density from the spectra and is a standard procedure for real eigenvalues, but it is more delicate in the complex case. It is convenient to introduce the complex ratios

$$z_j = \frac{\lambda_j - \lambda_j^{nnn}}{\lambda_j - \lambda_j^{nn}} = r_j e^{i\theta_j}, \quad (8)$$

where λ_j^{nnn} is the next-to-near neighbor of λ_j in the complex plane. This removes the dependence on the local

Quantum spin chains with local interactions and local coupling to the environment		
XXZ Hamiltonian with next-nearest neighbor coupling $\hat{H}(J_1, J_2, \Delta)$		
Lindblad operators	$\hat{L}_j^{(0)} = \sqrt{\gamma_0} \hat{\sigma}_j^z$	$\hat{L}_j^{(1)} = \sqrt{\frac{\gamma_1}{2}} (\hat{\sigma}_j \cdot \hat{\sigma}_{j+1} + 1)$
$\hat{L}_j^{(2)} = \sqrt{\gamma_2} \hat{\sigma}_j^+ \hat{\sigma}_{j+1}^-$	$\hat{L}_j^{(3)} = \sqrt{\gamma_2} \hat{\sigma}_j^- \hat{\sigma}_{j+1}^+$	
Model (A)	$\gamma_1 = \gamma_2 = 0$	Integrable with decoupled BBGKY hierarchy at $J_2 = \Delta = 0$
Model (B)	$J_1 = J_2 = 0, \gamma_0 = \gamma_2 = 0$	BBGKY hierarchy does not decouple; Integrable for $\Delta = 0$
Model (C)	$J_2 = \Delta = 0, \gamma_1 = 0$	dissipative freezing
Model (D)	$J_2 = \gamma_0 = \gamma_1 = 0$	Non-integrable; BBGKY hierarchy decouples for $\Delta = 0, \gamma_2 = \gamma_3$;

TABLE II. The many-body case is represented by different variants of the XXZ Hamiltonian in the presence of next-neighboring hopping and different instances of local and correlated dissipation. The four Models (A)-(D) represent different cases where ergodicity is broken for different reasons (integrability, fragmentation) or because the BBGKY hierarchy decouples. Model D is integrable with operator-space fragmentation for $J_1 = \Delta = 0$

density and implicitly unfolds the spectrum [59]. Under the hypotheses of Poisson/Ginibre spectra, the distribution of z_j visibly changes, as the level repulsion results in a suppression of the probabilities of finding z_j close to the origin of the plane and θ close to 0. An example of this difference is shown in Fig. 2, where we apply this criterion to identify regular and chaotic regimes of a dissipative quantum top analyzed further in Sec. V. A simple quantitative way to quantify the distinction is to calculate the average $\cos \theta$, equal to 0 in the Poisson case, and $\cos \theta \approx -0.24$ for the Ginibre ensemble.

B. Lindblad BBGKY hierarchy

A particularly simple class of models with operator space fragmentation are Lindblad equations with decoupled BBGKY hierarchies for the equations of motion for correlation functions. These exhibit significant simplifications in their dynamics, which are a priori not related to integrability. Their structure is most easily explained by considering models of spinless fermions with creation annihilation operators c_i^\dagger, c_j that fulfil $\{c_i^\dagger, c_j\} = \delta_{ij}$. The expectation value of a generic observable O evolves under the adjoint equation

$$\frac{d}{dt} \langle O \rangle = i \langle [H, O] \rangle + \sum_{\alpha} \gamma_{\alpha} \left(\langle L_{\alpha}^\dagger O L_{\alpha} \rangle - \frac{1}{2} \langle \{ L_{\alpha}^\dagger L_{\alpha}, O \} \rangle \right).$$

The operators $O_{\{i\},\{j\}}^{n,m} = c_{i_1}^\dagger \dots c_{i_n}^\dagger c_{j_1} \dots c_{j_m}$ form a basis and obey an infinite hierarchy of coupled equations of

motion

$$\frac{d}{dt} \langle O_{\{i\},\{j\}}^{n,m} \rangle = \sum_{\{k\},\{l\}} \mathcal{K}_{r,s}^{n,m} (\{i\},\{j\}|\{k\},\{l\}) \langle O_{\{k\},\{l\}}^{r,s} \rangle,$$

where the kernels \mathcal{K} follow from (III B). When the set of jump operators is closed under conjugation, $\{L_{\alpha}^\dagger\} = \{L_{\beta}\}$, the (adjoint) dissipator can be written as a double commutator

$$\frac{d}{dt} \langle O_{\{i\},\{j\}}^{n,m} \rangle_t = i \langle [H, O_{\{i\},\{j\}}^{n,m}] \rangle_t - \frac{1}{2} \sum_{\alpha} \langle [L_{\alpha}^\dagger, [L_{\alpha}, O_{\{i\},\{j\}}^{n,m}]] \rangle_t. \quad (9)$$

If we assume that both the Hamiltonian and the jump operators are quadratic in the fermionic operators, the equations above preserve the number of fermions: an operator can only mix with others carrying the number of fermion creation/annihilation operators, resulting in a decoupling of the hierarchy of correlation functions [47]. This structural simplicity has been used to obtain exact results in non-integrable Lindblad models [48–51], and it is natural to ask whether an appropriate measure of complexity could serve as a witness of this dynamical simplification.

IV. QUANTUM TRAJECTORIES AND THEIR INTRINSIC DIMENSION

Open quantum systems can be described by unravelling their master equation into QT. This entails defining

a stochastic evolution on the Hilbert space, in such a way that averaging over the realizations of the stochastic process recovers the dynamics of the density matrix. A single realization of the stochastic evolution is called a *quantum trajectory*. Unraveling has been proven to be a very useful numerical tool for the integration of Lindblad equations and is also experimentally relevant, since it accounts for the dynamics of quantum systems subject to monitoring [67–69]. Physical properties of QT have recently attracted attention, fueling studies for instance on their thermodynamics [103–106] and on measurement-induced phase transitions [107–109]. The aim of this paper is to investigate whether QT inherit any property from the dynamical structure of the associated Lindbladian. In particular, we will analyze their complexity as quantified by their intrinsic dimension. Such a correlation is not a priori expected for integrable Lindblad equations, because weak symmetries do not typically imply the existence of conservation laws that constrain QT [96, 101].

There is an infinite number of ways to unravel the Lindblad equation. Below we discuss the quantum jump unraveling and the corresponding trajectories. Afterwards we will explain their data set representations and introduce the intrinsic dimension as a measure to quantify their complexity.

A. Quantum jumps

Quantum jump unravelings arise experimentally, for example, from photon-counting processes: the system is coupled to a monitoring apparatus, and evolves deterministically until the detector measures a photon that was entangled with the system, inducing a sudden collapse of its wavefunction called quantum jump [68]. The jump occur at random times and the dynamics is described by the stochastic process illustrated below (consider for simplicity an initial pure state $|\psi_0\rangle$). For each time increment dt , the wavefunction evolves as $|\psi_t\rangle \rightarrow |\psi_{t+dt}\rangle$, with

$$|\psi_{t+dt}\rangle = \begin{cases} \frac{L_\alpha |\psi_t\rangle}{\|L_\alpha |\psi_t\rangle\|} & \text{with probability } p_\alpha \\ \frac{e^{-i dt H_{\text{eff}}} |\psi_t\rangle}{\|e^{-i dt H_{\text{eff}}} |\psi_t\rangle\|} & \text{with probability } p_0 \end{cases} \quad . \quad (10)$$

In Eq.(10), $p_\alpha = dt \langle \psi_t | L_\alpha^\dagger L_\alpha | \psi_t \rangle$, $p_0 = 1 - \sum_\alpha p_\alpha$, and the non-Hermitian Hamiltonian $H_{\text{eff}} = H - \frac{i}{2} \sum_\alpha L_\alpha^\dagger L_\alpha$. The non-Hermitian term in H_{eff} ensures the conservation of probability in the evolution. Each realization of the stochastic process is characterized by the sequence $n \equiv \{(t_1, \alpha_1); (t_2, \alpha_2); \dots, (t_n, \alpha_n); \dots\}$ with $t_i \in [0, T]$. The mean state is defined as the average over all possible QTs $\rho_t \equiv \text{En}[|\psi_t\rangle n n \langle \psi_t|]$. It is straightforward to show that ρ_t evolves according to the Lindblad equation

in Eq.(4). While averages of observables can be equivalently computed through QTs or the Lindblad evolution, non-linear functionals of the state, such as higher moments $\text{En}[(|\psi_t\rangle n n \langle \psi_t|)^k]$, are not predicted by the Lindblad equations, indicating that QT actually encode more information than the Lindblad equation. The intrinsic dimension defined in the next subsection, the key quantity for our characterization of the complexity of QTs, is a non-linear function of the state.

B. Intrinsic dimension

The intrinsic dimension I_d is a quantifier of the minimal number of independent parameters that are necessary to characterize a given data set without significant loss of information. An abstract data set can be represented by a sequence of vectors $\{x_i\}_{i=1\dots N}$, where $x_i \in \mathbb{R}^D$ and D is called the *embedding dimension*. The embedding dimension depends on how data points are represented: a sub-optimal encoding of the information contained in the points would result in an inefficient representation. As a result of correlations, data points are often restricted to a submanifold of \mathbb{R}^D , and the intrinsic dimension is defined as the dimensionality of this submanifold. This is a typical property of complex data sets: an example in Physics is that while ground states of many-body quantum systems are mathematically represented as vectors in a high-dimensional Hilbert space, they often allow for compressed representations exploiting their entanglement structure.

The estimation of I_d is an active field of research and there are many approaches to it, each with its own advantages and disadvantages [74]. The definition given above is not practical, since the embedding manifold is a priori unknown and the I_d must be inferred from the correlations of a discrete set of points. The correlation dimension introduced by Grassberger and Procaccia for fractals [110] is a suitable estimator, but suffers from a density dependence problem. Other relevant approaches involve principal component analysis (PCA), multi-dimensional

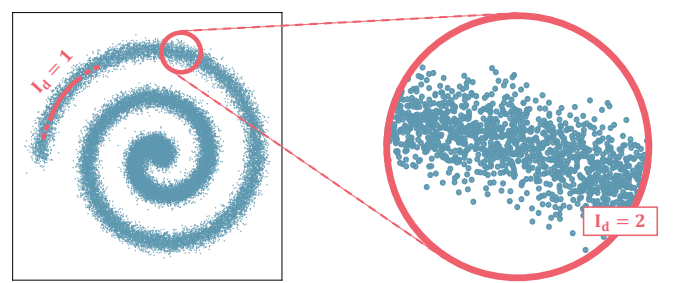


FIG. 1. Illustration of the scale dependence of the intrinsic dimension. If the nearest neighbours lie at a distance comparable to the scale of local noise, the structure appears two-dimensional. Only at an appropriately large scale the underlying curve emerges.

scaling (MDS) methods, neural networks [111–115]. We focus on the **2-NN method**, which estimates I_d using the distances to the first and second nearest neighbors of each data point. We briefly describe the algorithm, referring the reader to the original paper for a more detailed discussion [81]. Given a distance function d on the embedding space, for each data point x_i one calculates the distance to its nearest neighbor $r_i^{nn} = d(x_i, x_i^{nn})$ and to its next-to-nearest neighbor $r_i^{nnn} = d(x_i, x_i^{nnn})$. One then defines the ratio $\mu_i = r_i^{nnn}/r_i^{nn} \geq 1$, which removes the influence of different densities in distinct regions of the data set. Assuming that the neighbors reside in a small ball with dimension $I_d \leq D$ where points are uniformly distributed (formally from an I_d -dimensional Poisson process), the ratios μ follow a Pareto distribution $p(\mu) = I_d \mu^{-I_d-1}$. Its cumulative distribution function $F(\bar{\mu}) \equiv \text{prob}\{1 \leq \mu \leq \bar{\mu}\}$ satisfies

$$-\log[1 - F(\mu)] = I_d \log \mu, \quad (11)$$

which implies that I_d can be estimated from a simple linear regression of $\{(\log \mu_i, -\log[1 - \hat{F}(\mu_i)])\}_{i=1,\dots,N}$, where \hat{F} is the empirical cumulative distribution function. The assumption of uniformity is important, but mild, because the data set only needs to be *locally* uniform on the scale of nearest-neighbors. In practice, one can check that this hypothesis is satisfied from the accuracy of the linear fit described above: real data sets typically show some minor deviations, and the regression is then performed over the linear region [81].

An important fact to note is that I_d is scale dependent. This behavior can be easily explained by looking at toy examples. Consider a simple data set embedded in \mathbb{R}^2 constructed by sampling points from a 1d curve and adding some Gaussian noise, *cf.* Fig. 1. On short scales the noise spreads the data points in the plane, resulting in a two-dimensional data set. However, on scales that are large compared to the variance of the noise the underlying curve emerges. The scale that the **2-NN** method probes can be quantified by the typical nearest-neighbor distance $\bar{r} = 1/2 \cdot \overline{r^{nn} + r^{nnn}}$, where the bar denotes the average over the data set. In the previous example $I_d = I_d(\bar{r})$ would be a decreasing function, but the opposite behavior is also possible. For example, the data set obtained by sampling points from a space filling curve such as the Hilbert curve would appear two-dimensional if the points are not too dense, while on shorter scales the underlying one-dimensional structure becomes evident. In general, studying the scale dependence of I_d provides complementary information on the data manifold [81, 116–118].

C. Quantum trajectories as data sets

We start from a fixed, randomly chosen initial pure state $|\psi_0\rangle$. Given a set of N QT $|\psi_t\rangle_{n_i}$, $i = 1, \dots, N$ at least two meaningful intrinsic dimensions could be

considered. The first is the I_d of individual QT. Every trajectory is a piecewise continuous curve (with discontinuities possibly arising at jump times), therefore intrinsically one-dimensional. However, akin to what happens with classical dynamical systems and chaotic attractors, one-dimensional trajectories can be space-filling and cover a higher-dimensional portion of the Hilbert space, as we will show in Section V. In this case, the data set associated to the i -th trajectory is $\mathcal{D}_i \equiv \{|\psi_0\rangle, |\psi_{dt}\rangle_{n_i}, |\psi_{2dt}\rangle_{n_i}, \dots\}$, up to a final time that is long enough to stabilize the result. To perform the analysis described in Section IV B, we have to store the information contained in wavefunctions –naturally living in a complex Hilbert space \mathcal{H} – in real vectors. For most of this work, we choose to do so by separating the real and imaginary parts of each of their components; as a consequence, the embedding space that we employ is \mathbb{R}^D , $D = 2 \dim \mathcal{H}$. Other possibilities exist: for instance one could represent the quantum state by storing expectation values of Hermitian observables. Indeed, this is what we will employ in Fig. 4, where we consider individual trajectories represented only by few expectation values, in order to build an intuition.

The rest of our analysis will be dedicated to the intrinsic dimension of the entire set of trajectories as a function of time: at a given time t , different QT reach different points spread out in the Hilbert space, and we estimate the dimensionality of the structure they are covering. To estimate I_d at a time t we consider the data set

$$\mathcal{D}_t \equiv \{|\psi_t\rangle_{n_1}, |\psi_t\rangle_{n_2}, \dots, |\psi_t\rangle_{n_N}\} \quad (12)$$

and the nearest-neighbors are classified according to the Euclidean distance of the normalized wavefunctions

$$d(\psi, \phi) = \sqrt{\|\psi - \phi\|^2}. \quad (13)$$

We then compute $I_d(t) = I_d[\mathcal{D}_t]$ at several times t in order to observe the evolution of the complexity of QT. The advantages of this approach are twofold. First, it provides us with a single, time-dependent measure of complexity that is not associated with individual trajectories. Second, the points used to construct the data sets are uncorrelated in time, which removes the influence of the underlying one-dimensional structure of individual trajectories. This results in a more direct applicability of the Pareto assumption. A disadvantage of this approach is its higher computational cost, which arises because the calculation of I_d cannot be run in parallel for every individual trajectory. In Appendix B we compare the results obtained from the two methods.

V. DRIVEN-DISSIPATIVE QUANTUM TOP

A prototypical model of quantum chaos is the kicked top, which has been extensively studied in the context of closed, unitary systems (e.g. [119–127]). The effects of dissipation on spectral statistics were investigated in [54].

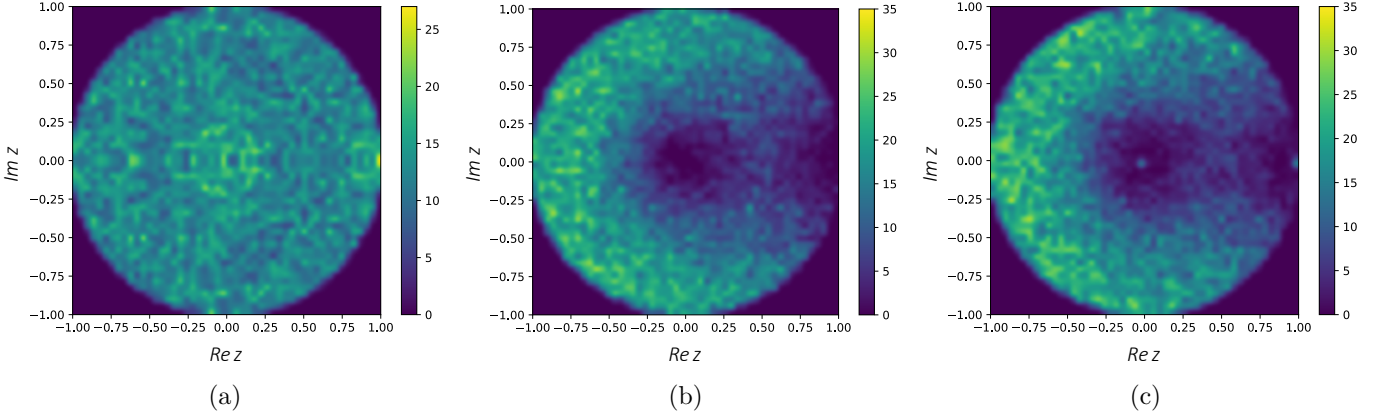


FIG. 2. Complex ratios of the GHS kicked top with parameters $S = 80$, $\omega_z = 4$, $g = 5$, in the regular and chaotic regimes: (a) $\omega_x = 0$, $k = 0$, $\gamma = 0.2$ (integrable); (b) $\omega_x = 0$, $k = 4$, $\gamma = 4$ (with kicks); (c) for $\omega_x = 2$, $k = 0$, $\gamma = 2$. The level repulsion is well captured by the angular distributions, having (a) $\cos \theta = 0.001$, (b) $\cos \theta = -0.23$, (c) $\cos \theta = -0.24$.

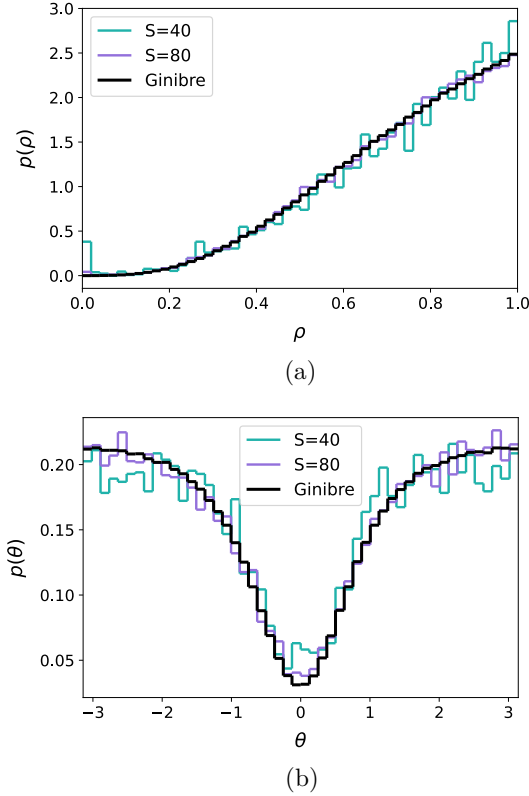


FIG. 3. (a) Radial and (b) angular distributions corresponding to Fig. 2 (c), showing the convergence of the complex ratios to chaotic spectral statistics. The reference distributions are obtained by sampling $S = 200$ $N \times N$ random matrices with size $N = 10000$ from the Ginibre ensemble.

We begin our analysis revisiting the results of Ref. [54] and extending them to a case where chaotic dynamics emerges purely from quantum fluctuations. We start by

recalling the form of the Hamiltonian, *cf.* Eq. 1

$$\hat{H}(\omega_z, g, \omega_x, k) = \hat{H}_0 + \sum_{n=-\infty}^{\infty} \delta(t - n\tau) \hat{H}_k,$$

with $\hat{H}_0 = \omega_z \hat{S}_z + (g/S) \hat{S}_z^2 + \omega_x \hat{S}_x$ and $\hat{H}_k = (k/S) \hat{S}_y^2$.

The top is subject to a periodic driving, chosen for simplicity as impulsive kicks at times $t = n\tau$. It is well-known that the top can be viewed as a model of many spins undergoing infinite-range collective processes by identifying the operators \hat{S}_α with the components of the total angular momentum operator of $N = 2S$ individual spins 1/2. In this case the $1/S$ scaling with the total spin is the Kac factor of the associated long-range model [128]. Thanks to this representation the model can experimentally realized for instance with cold atoms [123] or superconducting qubits [124]. In the large- S limit, the spectral statistics of the Hamiltonian in Eq. (1) exhibits a crossover from Poisson to Wigner-Dyson as the kick strength k is increased, which is a signature of unitary quantum chaos [119]. Another important property is that the quantum top becomes semiclassical when the spin S is large, *cf.* Appendix A. In this limit, $1/S$ acts as an effective Planck's constant that bounds quantum fluctuations. In agreement with the BGS conjecture, the presence of chaos signaled by the spectral statistics mirrors the emergence of chaos in the limiting classical model, whose phase space displays growing chaotic regions in presence of driving [53, 102].

We now introduce dissipation through a jump operator $\hat{L} = \sqrt{\gamma} \hat{S}_-$. This gives rise to the Lindblad equation

$$\frac{d\hat{\rho}}{dt} = -i[\hat{H}, \hat{\rho}] + \frac{\gamma}{S} \left(\hat{S}_- \hat{\rho} \hat{S}_+ - \frac{1}{2} \{ \hat{S}_+ \hat{S}_-, \hat{\rho} \} \right). \quad (14)$$

Both the Hamiltonian and the dissipator commute with the total angular momentum $\hat{S}^2 = \hat{S}_x^2 + \hat{S}_y^2 + \hat{S}_z^2$, which therefore defines a strong symmetry, and the dynamics takes place in a subspace with conserved spin. The presence of dissipative chaos can be detected by analyzing the

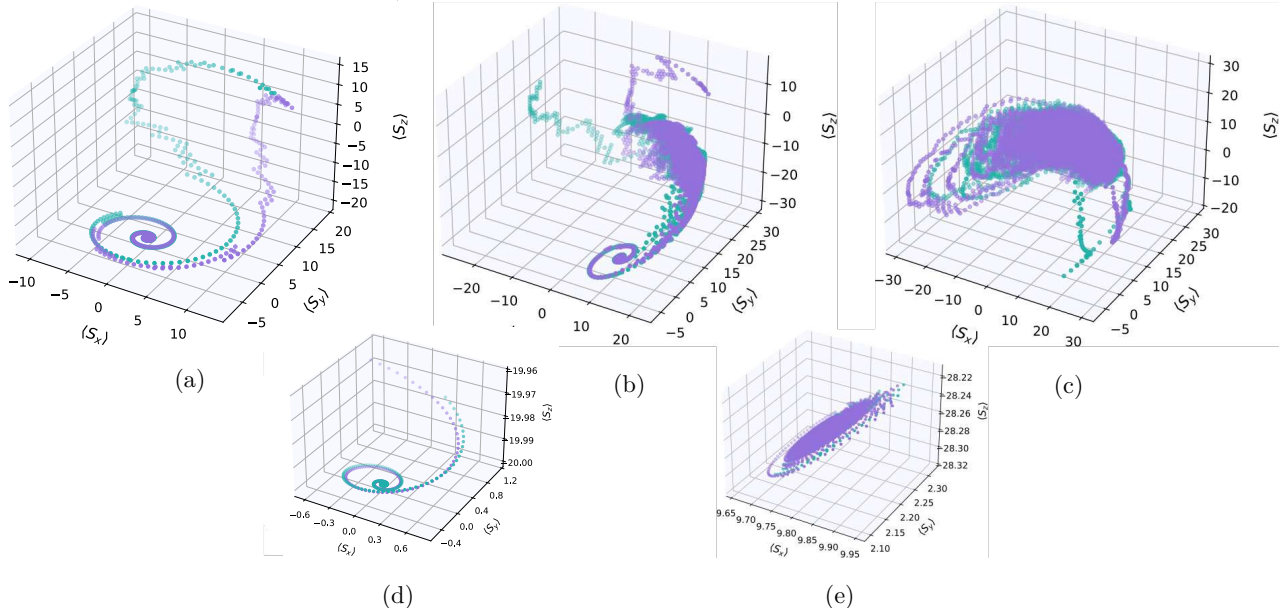


FIG. 4. Chaotic behavior of the dissipative quantum top as seen from individual QT. We plot two QT of the model given by Eq. (14) with $\omega_z = 1$, $g = 5$, $k = 0$, considering in (a), (b) $\omega_x = 0$, in (c), (d) $\omega_x = 3$ and in (e) $\omega_x = 5$. Even if trajectories are always perturbed by stochastic effects, the local structure between consecutive quantum jumps is one-dimensional in the integrable case (a). The subfigure (d) is a zoom on the spiraling region at the end of the trajectories in (a), showing that different trajectories are attracted towards the same one-dimensional region. Increasing ω_x , a transient chaotic region starts to appear, where the trajectories get trapped before escaping to another long-time attractor. As shown in (e), this structure is not one-dimensional, in contrast to the integrable case. For sufficiently large values of ω_x , the chaotic attractor takes over, as we depict in (e). The appearance of initially small chaotic regions that become dominant increasing the integrability-breaking coupling is reminiscent of what happens in the classical systems, where chaotic trajectories take over the phase space.

spectrum of the Lindblad generator, as discussed in Section III A. For a Floquet model like Eq. (1), one studies the eigenvalues of the stroboscopic time-evolution operator. Vectorizing the Eq. (14) leads to

$$\check{\mathcal{L}} \equiv \check{\mathcal{L}}_0 + \sum_{n=-\infty}^{\infty} \delta(t - n\tau) \check{\mathcal{L}}_k, \quad (15)$$

where $\check{\mathcal{L}}_0 = -i\check{\mathcal{H}}_0 + \check{\mathcal{D}}$ includes the time-independent part of the Hamiltonian and the dissipator, while $\check{\mathcal{L}}_k = -i\check{\mathcal{H}}_k$ only the kicks. Defining $|\rho(t+\tau)\rangle\rangle = \hat{\mathcal{F}}_\tau|\rho(t)\rangle\rangle$, the evolution operator for a single period is

$$\hat{\mathcal{F}}_\tau = e^{\tau\hat{\mathcal{L}}_0} e^{\hat{\mathcal{L}}_k} = e^{\tau(\hat{\mathcal{D}} - i\hat{\mathcal{H}}_0)} e^{-i\hat{\mathcal{H}}_k}. \quad (16)$$

We focus on two scenarios:

- We fix $\omega_x = 0$ and vary the kick strength k .
- We set $k = 0$ and tune ω_x .

The corresponding distributions of the complex ratios defined in Eq. (8) are reported in Fig. 2. When $k = 0$ and $\omega_x = 0$ the model is integrable [129] and correspondingly shows signatures of 2d-Poisson statistics, *cf.* Fig. 2 (a). Adding kicks leads to chaotic behavior and complex ratio distributions described by the Ginibre ensemble, *cf.* Fig. 2 (b) and (c). This was first studied in Ref. [61],

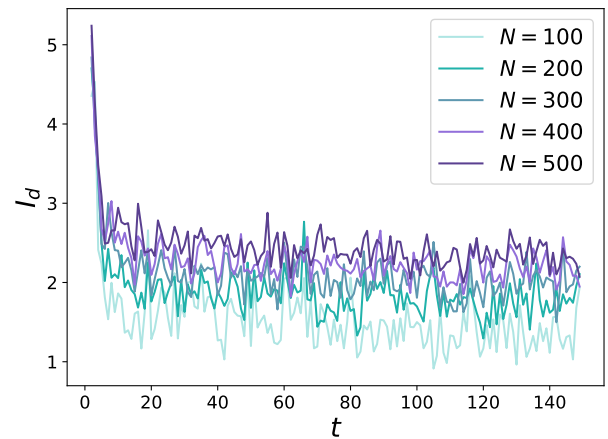


FIG. 5. Time evolution of the intrinsic dimension for the dissipative top with $\omega_z = 1$, $g = 5$, $\omega_x = 4.0$, $k = 0$ and $\gamma = 2$, $S = 30$. The value of $I_d(t)$ is estimated using different different numbers of trajectories, encoding now the scale dependence of I_d . With a larger N , the points are on average closer to each other and probe a finer scale of the data set, resulting in increasing values like for the I_d calculated along individual trajectories.

where the Poisson-to-Ginibre crossover, on increasing S ,

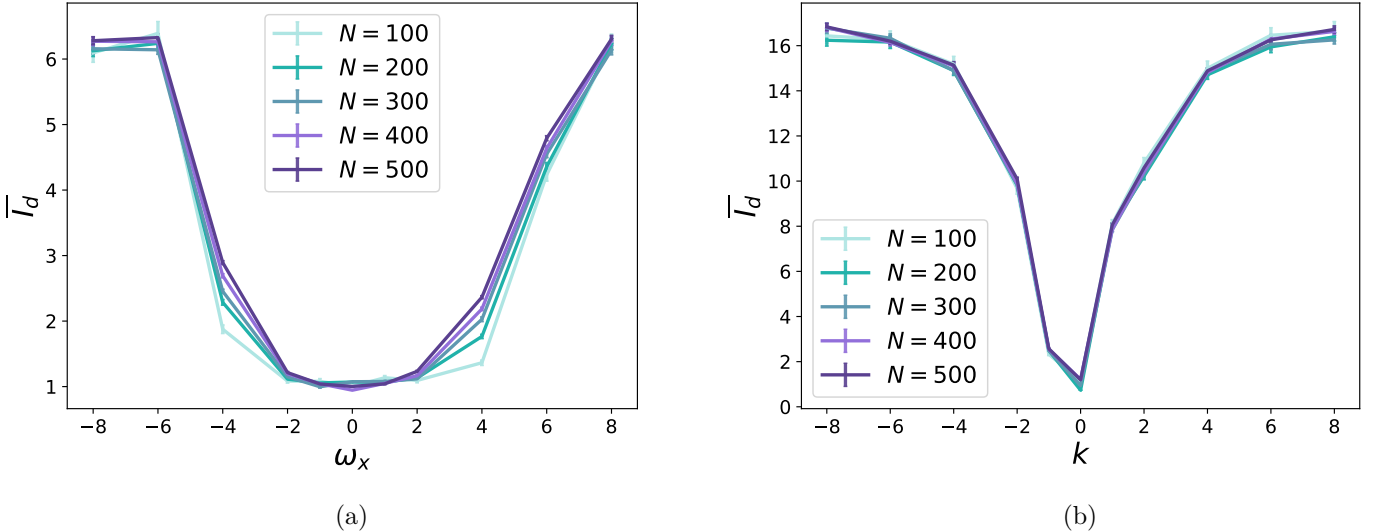


FIG. 6. Late-time average of $I_d(t)$ for the dissipative top with $\omega_z = 1$, $g = 5$, $\gamma = 2$ and $S = 30$, varying respectively ω_x and k in (a), (b). The error bars shown represent the standard deviation of $I_d(t)$ for late times. The integrable point of the quantum top is associated to one-dimensional trajectories; when chaos is present the I_d increases in a model dependent manner.

was associated with the emergence of chaos as the kick strength k is increased.

Including ω_x makes the model quantum chaotic without introducing chaos in its classical limit. As we describe in greater detail in the Appendix A, the classical limit of Eq. (14) is a dynamical system on the 2-sphere, and, in absence of kicks, chaos is topologically forbidden by the Poincaré-Bendixson theorem. Only the inclusion of a driving term can generate chaotic orbits [65, 66]. The corresponding distribution of the eigenvalues shows signatures of chaos, even when the behavior of the classical limit remains regular, therefore providing an exception to the GHS conjecture. We include in Fig. 3 the radial and angular distributions to further support our claims. This result also implies that a direct quantum analog of the Poincaré-Bendixson theorem does not exist. Our observations are corroborated by recent literature [56, 57], which support the idea that in open systems quantum chaos can arise even in the absence of its classical counterpart.

Before calculating the intrinsic dimension, it is instructive to consider the trajectories on the 3d space spanned by the expectation values $\langle \hat{S}_\alpha \rangle$, $\alpha = x, y, z$ evaluated in a single QT, as shown in Fig. 4. For parameter values corresponding to integrable Lindblad equations the underlying one dimensional structure of these trajectories is evident. For values of t between consecutive quantum jumps the discrete points $\langle \hat{S}_\alpha \rangle_t$ are aligned along a curve, even though there are random discontinuities introduced by the jumps. When quantum chaos is present according to the complex level spacing analysis, the trajectories appear to “fold upon themselves” and the time series of $\langle \hat{S}_\alpha \rangle_t$ fills a region of higher dimensionality of the space. Remarkably, this feature is present when chaos is introduced by kicks as well as

and when H is kept time-independent, in agreement with the spectral statistics but not with the classical limit. Counterexamples to the GHS conjecture have been employed in the literature to question the validity of the level-spacing statistics criterion for dissipative chaos [57]. Our results instead support the picture arrived at by means of the level-spacing statistics analysis, indicating that it is the quantum-classical correspondence that fails in this regime. This happens because the regular classical dynamics can describe the model at finite S only up to some time scale analogous to the Ehrenfest time. Beyond that, the $O(1/S)$ fluctuations bring the state in a fully quantum regime, where the complete spectrum has a significant influence on the dynamics.

The expectation values $\langle \hat{S}_\alpha \rangle_t$ only provide a small part of the information encoded in the QT. To understand whether the structure of chaotic trajectories is intrinsically higher-dimensional we have to consider the data set formed by the full QT $|\psi(t)\rangle \in \mathcal{H}$. As wave functions in a high-dimensional Hilbert space cannot be easily visualized we focus on calculating the intrinsic dimension. As discussed in Sec. IV C, we calculate I_d as a function of time using the data sets $\mathcal{D}_t \equiv \{|\psi_t\rangle_{n_1}, |\psi_t\rangle_{n_2}, \dots, |\psi_t\rangle_{n_N}\}$, consisting of the states of each of the N trajectories at the same time t . The results are shown in Fig. 6. As we have seen in Fig. 4, at early times trajectories spread over the Hilbert space along independent directions. This corresponds to the initial large- $I_d(t)$ regime in Fig. 5. At later times, the trajectories get trapped in a complex subset of \mathcal{H} , that could be interpreted as an attractor. At any sufficiently late time t , the points $\{|\psi_t\rangle_{n_i}\}$ are randomly drawn from this subset, implying that we can obtain an estimate of

the dimensionality of the attractor as a late time average

$$\bar{I}_d = \frac{1}{|T - \bar{t}|} \int_{\bar{t}}^T I_d[\mathcal{D}_t] dt, \quad (17)$$

where $I_d[\mathcal{D}_t]$ is estimated from Eq. (11) and \bar{t} is the time at which its values become stationary. In Fig. 6 we show the results for \bar{I}_d as functions of ω_x and k . The results corroborate the intuitive picture suggested by the time evolution of the expectation values $\langle \hat{S}^\alpha \rangle$: close to the integrable point we estimate $\bar{I}_d \approx 1$ and the intrinsic dimension increases as we increase integrability-breaking couplings, meaning that individual QT describe a data manifold with increasing complexity. Including in the model further dissipation channels induced by \hat{S}_+ or \hat{S}_z would not break integrability [129], and the associated QT remain one-dimensional. Also the fluctuations, measured by the standard deviation of the late-time values of I_d , are very small when the model is integrable.

A word of caution is needed by analyzing the data in Fig. 6. Despite the fact that at the integrable point the intrinsic dimension is minimal, its growth is rather smooth on increasing the integrability-breaking term (see the behavior in the true many-body case discussed in the next Section). We expect that in the case of the quantum top, due to the polynomial increase of Hilbert space dimension with S , finite-size effects are more severe and one should go to much larger S to see a sharpening of the curves around the integrable point.

Increasing the spin S of the quantum top leads to a larger embedding space with real dimension $D = 4S + 2$. However, it is interesting to note that the intrinsic dimension of this model does not increase with S , within the range of values that we have considered. When $\omega_x = 0$, $k = 0$ one obtains $I_d \approx 1$ independently of the value of the spin, while for a stronger chaotic coupling the I_d is a weakly decreasing function of S , as shown in Fig. 7. Calculating the I_d along single trajectories gives results consistent with the above analysis, as discussed Appendix B. In the autonomous case, we observe a finite interval of ω_x over which I_d remains statistically compatible with 1. Consequently, at finite system size the intrinsic dimension alone does not allow us to fully rule out residual integrable effects for sufficiently small ω_x , even though the minimal mean value occurs at the expected integrable point $\omega_x = 0$. The values of I_d show a tiny variation with the number of trajectories, especially at non-integrable points. This is an effect of the scale dependence of the intrinsic dimension, that we study in detail in Appendix C.

VI. QUANTUM SPIN CHAINS WITH DISSIPATION

We now turn to the case of genuine many-body models using variations of the spin-1/2 Heisenberg XXZ chain with dissipation as our testing ground. This will allow us

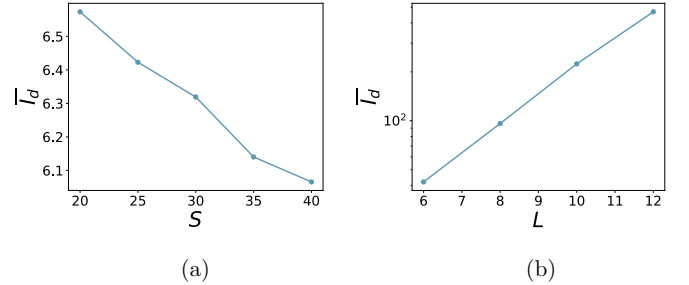


FIG. 7. Dependence of I_d on the Hilbert-space dimension: In (a) Chaotic quantum top with $\omega_x = -8.0$ and different spin values; (b) Model (A) $\Delta = 1.0$ (note the logarithmic scale).

to study the effects of quantum integrability, the decoupling of the open system analog of the BBGKY hierarchy for correlation functions and strong symmetries on the intrinsic dimension of QT.

A. Models

We start by recalling the models introduced in Table II. The many-body models we consider in the following are summarized in TABLE II. Their unitary terms are particular cases of the spin-1/2 Hamiltonian in Eq. (3)

$$\begin{aligned} \hat{H}(J_1, J_2, \Delta) = & \sum_{j=1}^{L-1} J_1 \left[\hat{\sigma}_j^x \hat{\sigma}_{j+1}^x + \hat{\sigma}_j^y \hat{\sigma}_{j+1}^y \right] + \Delta \hat{\sigma}_j^z \hat{\sigma}_{j+1}^z \\ & + J_2 \sum_{j=1}^{L-2} \left(\hat{\sigma}_j^x \hat{\sigma}_{j+1}^x + \hat{\sigma}_j^y \hat{\sigma}_{j+1}^y \right). \end{aligned} \quad (18)$$

For $J_2 = 0$ this reduces to the integrable spin-1/2 Heisenberg XXZ chain. The Lindblad equations are chosen by combining (18) with specific choices of jump operators:

- Model A: Local dephasing

$$\hat{L}_j^{(0)} = \sqrt{\gamma_0} \hat{\sigma}_j^z. \quad (19)$$

The resulting Lindblad equation is non-integrable as can be verified by a spectral statistics analysis [58, 59], except at the special point $\Delta = 0$ and $J_2 = 0$. Yang-Baxter integrability at $(\Delta, J_2) = (0, 0)$ has been proven by constructing the vectorized representation of the Lindbladian, which becomes a non-Hermitian, integrable Fermi-Hubbard model with imaginary interaction proportional to $i\gamma_0$ [30]. At the integrable point $(\Delta, J_2) = (0, 0)$ the model features a decoupled BBGKY hierarchy as well. Tuning J_2 away from zero retains this feature, while breaking integrability.

- Model B: $J_1 = J_2 = 0$ and jump operators

$$\hat{L}_j^{(1)} = \frac{\sqrt{\gamma_1}}{2} (\hat{\sigma}_j \cdot \hat{\sigma}_{j+1} + 1), \quad (20)$$

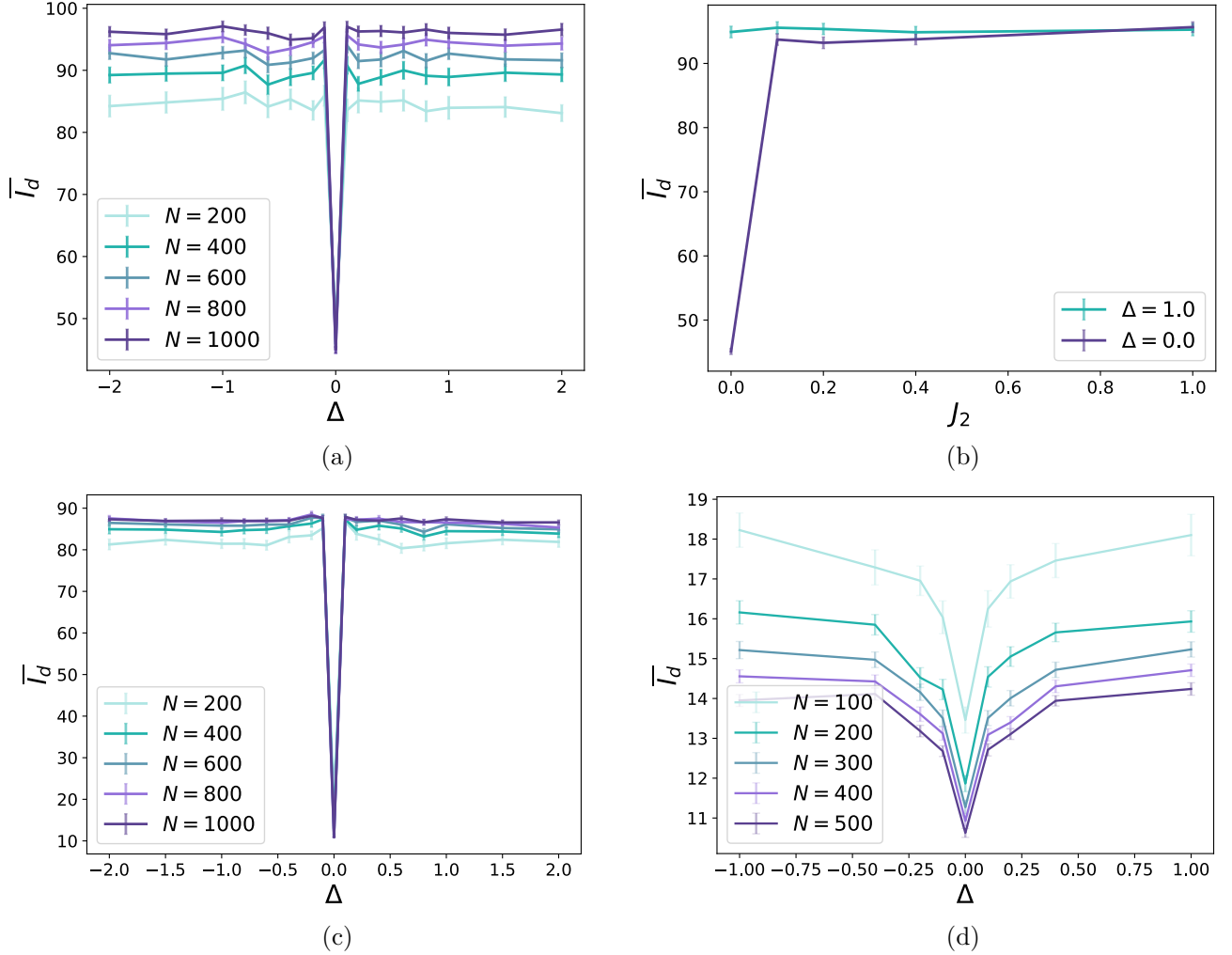


FIG. 8. Stationary intrinsic dimension \bar{I}_d obtained by averaging over N QT at late times for the many-body models described in TABLE II: (a) Model A with $J_1 = 1$, $\gamma_0 = 1$ for $L = 8$, as a function of Δ , with $J_2 = 0$. For $\Delta = 0$ the Lindblad equation is Yang-Baxter integrable. (b) Model A with $J_1 = 1$, $\gamma_0 = 1$ for $L = 8$, as a function of J_2 , with fixed $\Delta = 0.0, 1.0$ and computed for $N = 800$. For $\Delta = 0 = J_2$ the Lindblad equation is Yang-Baxter integrable. (c) Model B with $\gamma_1 = 1$. For $\Delta = 0$ the model is Yang-Baxter integrable. (d) Model D with $\gamma_2 = 1$ from a state with fixed spin. For $\Delta = 0$ the BBGKY hierarchy decouples.

where $\hat{\sigma} = (\hat{\sigma}_x, \hat{\sigma}_y, \hat{\sigma}_z)$. The purely dissipative model $\Delta = 0$ is known to be Yang-Baxter integrable [31], while $\Delta \neq 0$ breaks integrability.

- Model C: $J_2 = \Delta = 0$ and

$$\begin{aligned} \hat{L}_j^{(0)} &= \sqrt{\gamma_0} \hat{\sigma}_j^z \\ \hat{L}_j^{(2)} &= \sqrt{\gamma_2} \hat{\sigma}_j^+ \hat{\sigma}_{j+1}^- \\ \hat{L}_j^{(3)} &= \sqrt{\gamma_3} \hat{\sigma}_j^- \hat{\sigma}_{j+1}^+, \end{aligned} \quad (21)$$

This is relevant because, as we will see, changing the dissipator can have subtle effects related to a strong symmetry.

- Model D: $J_2 = \Delta = 0$ and

$$L_j^{(2)} = \sqrt{\gamma_2} \hat{\sigma}_j^+ \hat{\sigma}_{j+1}^- = (L_j^{(3)})^\dagger. \quad (22)$$

This corresponds to a generalization of the Quantum Symmetric Simple Exclusion Process [32, 130, 131], which is known to exhibit a decoupled BBGKY hierarchy [51].

B. Results

The picture that emerged in Section V is that the integrable points of the dissipative quantum top are characterized by an intrinsic dimension $I_d \approx 1$, which increases as chaotic behavior sets in. We now examine how these findings extend to more general settings, separating the discussion of the effects of integrability from those arising from the decoupling of correlation functions and dissipative freezing.

◦ Signatures of integrability

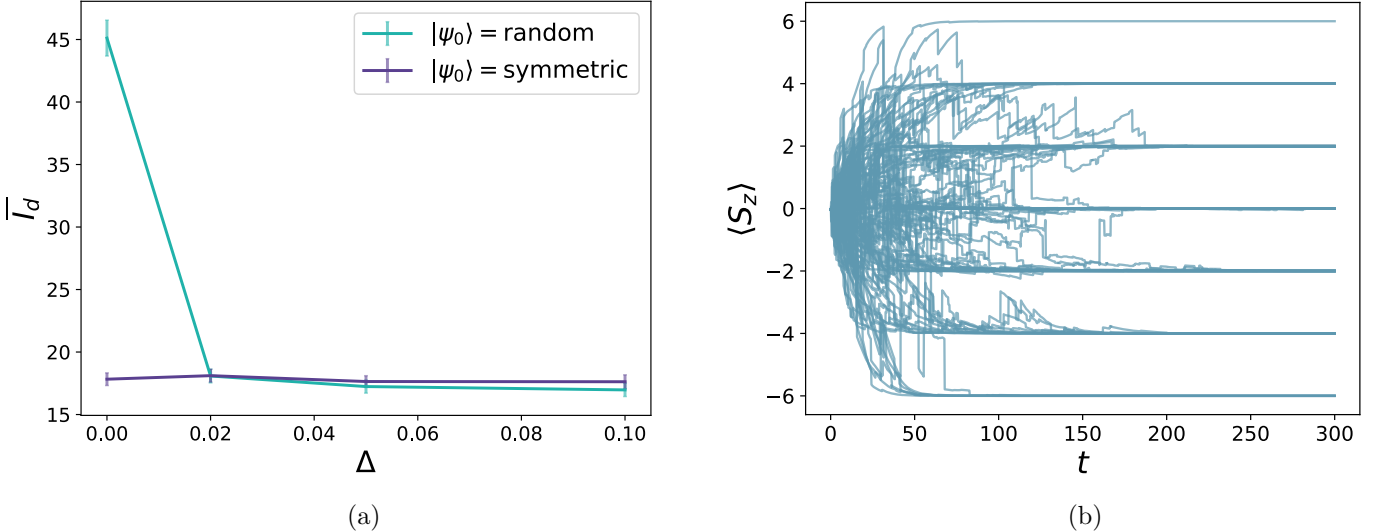


FIG. 9. Dissipative freezing mechanics as seen by: (a) the intrinsic dimension; (b) the expectation values of the charge.

We start from the XXZ chain subject to dephasing (Model (A)). QT are generated starting from a fixed random state, and we calculate the intrinsic dimensions as a function of time. The initial transient is generally faster and more difficult to access than in the single-body case, and $\bar{I}_d(t)$ fluctuates almost immediately around its late-time value. As shown in Fig. 8, the late-time average of the intrinsic dimension clearly indicates the presence of a quantum integrable point as the point of minimal complexity. We have investigated the evolution of \bar{I}_d to switching on either an exchange anisotropy Δ or a next-nearest-neighbor hopping J_2 , which respectively break the integrability of only the Lindbladian, and of both the Lindbladian and its Hamiltonian part. Both perturbations quickly drive \bar{I}_d to a constant larger value characteristic of the non-integrable regime. Note that this value is unaltered when Δ and J_2 are both switched on, indicating that \bar{I}_d does not simply react to any insertion of a new operator generating the dynamics.

This example of the XXZ chain highlights the importance of calculating the intrinsic dimension on the Hilbert space rather than focusing on a small number of expectation values along QT, *cf.* Fig. 4. The results shown in Fig. 8 are obtained for a short chain with $L = 8$ sites. The intrinsic dimension at the integrable point is $\bar{I}_d \approx 50$, which is much smaller than the embedding dimension $D = 2^9$, but still too large to be captured visually in a simple way. To fully exhibit the drop in complexity of QT by analyzing expectation values would require the identification of approximately 50 appropriately chosen operators, which is a highly nontrivial task in models without a simple classical limit.

In this case, increasing the length of the chain results in a larger embedding space with dimension $D = 2^{L+1}$, and, as reported in Fig. 7, the intrinsic dimension correspondingly increases exponentially for all values of Δ , showing no significant differences in the scaling law be-

tween integrable and non-integrable points.

The effects shown in Figs. 8 (a) and (b) could have their origin in integrability or BBGKY decoupling, since the correlation functions also decouple at $\Delta = 0$, $J_2 = 0$. To separate the effects of integrability and BBGKY decoupling we consider Model (B), which exhibits an integrable point with coupled hierarchy of correlation functions. In Fig. 8 (c) we show the results for \bar{I}_d as a function of the anisotropy parameter Δ . We see that \bar{I}_d drops sharply at the integrable point $\Delta = 0$. In contrast to the quantum top, at these integrable points \bar{I}_d is significantly larger than 1. This is expected, because in many-particle systems quantum integrability imposes only an extensive number of local constraints on the dynamics.

- *Signatures of BBGKY decoupling and dissipative freezing*

What we have observed so far does not exclude the possibility that the BBGKY decoupling by itself could affect the complexity of QT. Before specifically addressing this question, we gradually turn on the dissipator in Eq. (22) from the integrable XX chain with $\Delta = 0$, $J_2 = 0$ already subject to dephasing (Model (C)). As reported in Fig. 9, starting from a random state, we observe that adding a finite $\gamma_2 > 0$ sharply decreases the intrinsic dimension. At a first glance this result seems challenging to interpret, as γ_2 is an integrability-breaking coupling. This is caused by another effect that reduces the complexity of QT, which had been called *dissipative freezing* [96, 97]. This model has a strong $U(1)$ symmetry generated by the total magnetization $\hat{S}_z = \frac{1}{2} \sum_{j=1}^L \hat{\sigma}_j^z$, commuting separately with Hamiltonian and jump operators. Strong symmetries are associated with conservation laws on average and preserving $\text{tr}[\hat{\rho} \hat{Q}]$ for some charge Q is not sufficient to enforce the conservation law along individual trajectories. After a quantum jump in-

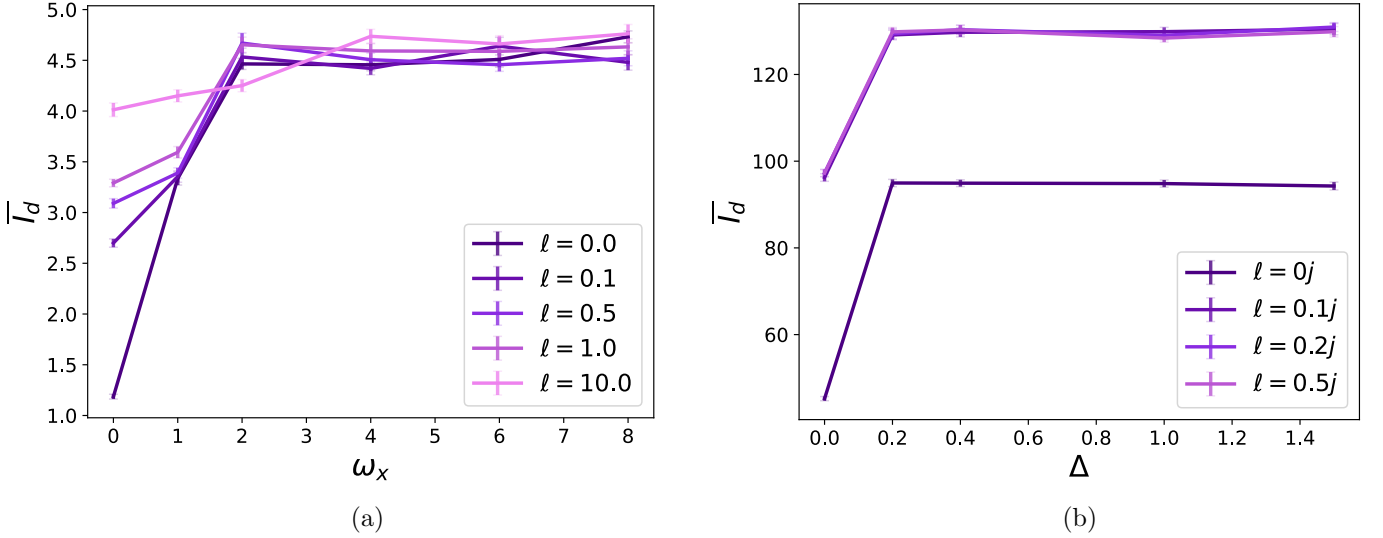


FIG. 10. Intrinsic dimension of quantum trajectories generated by different unravelings. The I_d is always calculated at fixed times. In (a) we consider the quantum top of Eq. (14) where integrability is broken by $\omega_x > 0$, and for simplicity we have taken ℓ real. The results for the XXZ chain with dephasing defined are presented in (b), where we have chosen instead an imaginary ℓ , because it resulted in a cleaner Pareto distributions.

duced by an operator \hat{L} , one has

$$\langle \hat{Q} \rangle_t \rightarrow \langle \hat{Q} \rangle_{t+dt} = \frac{\langle \psi_t | \hat{L}^\dagger \hat{Q} \hat{L} | \psi_t \rangle}{\langle \psi_t | \hat{L}^\dagger \hat{L} | \psi_t \rangle}$$

and $[\hat{L}, \hat{Q}] = 0$ is not sufficient in general to preserve the expectation values. Nevertheless, if $|\psi_t\rangle$ is an eigenstate of Q with eigenvalue q one obviously obtains $\langle Q \rangle_t = q = \langle Q \rangle_{t+dt}$, and analogously for the deterministic term. If a stochastic trajectory happens to hit an eigenstate, the dynamics gets trapped in the eigenspace and expectation values become frozen. While this may seem unlikely, it is actually expected to happen under generic conditions [96, 97]. Instead, the strong symmetry condition together with $(\hat{\sigma}^z)^2 = \mathbb{I}$ imply that dephasing quantum jumps are unable to modify the expectation values even if the state belongs to a superposition of eigenspaces. Adding $\gamma_2 > 0$ triggers the dissipative freezing, which becomes the main phenomenon witnessed by the intrinsic dimension, therefore hiding the effect of the BBGKY decoupling. To remove this spurious albeit interesting effect, we consider an initial state with fixed spin. We note that in the previous models we have considered this would only rescale all dimensionalities, since the dynamics becomes constrained in an eigenspace.

This brings us Model (D), with nearest-neighbor terms in the Hamiltonian and dissipation induced only by Eq. (22). As shown in Fig. 8, \bar{I}_d detects again the point with structurally simplified for dynamics with a local minimum at $\Delta = 0$, where the model exhibits a decoupled BBGKY hierarchy. We conclude that the intrinsic dimension of QT is able to witness the complexity of Lindblad dynamics, regardless of the mechanism driving the potential simplification.

VII. DEPENDENCE ON THE UNRAVELING

So far we have focused on the intrinsic dimension of quantum jump trajectories. Any Lindblad equation has infinitely many unravelings, it is therefore important to check whether our findings are a special property of quantum jumps, or if they are robust under modifications of the stochastic process. Consider the transformation

$$\hat{L}_\alpha \rightarrow \hat{L}_\alpha + \ell_\alpha, \quad (23a)$$

$$\hat{H} \rightarrow \hat{H} - \frac{i}{2} \sum_\alpha \gamma_\alpha \left(\ell_\alpha^* \hat{L}_\alpha - \ell_\alpha \hat{L}_\alpha^\dagger \right) + r, \quad (23b)$$

where $\ell_\alpha \in \mathbb{C}$ and $r \in \mathbb{R}$. This is a symmetry of the Lindblad equation Eq. (4), and the evolution of the mean state ρ is unaffected by the transformation. However, the stochastic processes defined by the quantum jump protocol over Eq. (23) are different, providing infinite unravelings of the same Lindblad equation. Other unravelings exist, such as homodyne or heterodyne QT (see Refs. [68, 69]). We focus on Eq. (23) because the parameters ℓ_α, r allow us to continuously deform the unraveling.

In Fig. 10 we show the intrinsic dimension for different unravelings for the quantum top and the XXZ chain with dephasing. For simplicity we have kept $r = 0$ and for the spin chain the unraveling has been modified considering $\ell_j = \ell$ equal at all sites. We see that the values of \bar{I}_d are in general unraveling-dependent, but for all cases considered the integrable point has always remained the point with minimal intrinsic dimension. Varying ℓ for the quantum top results in approximately constant intrinsic dimensions as long as the dynamics is chaotic. At the integrable point \bar{I}_d increases with ℓ , while the overall range of variation of \bar{I}_d with ω_x decreases. The behav-

ior for the dissipative XXZ chain shows some interesting differences. Taking $\ell \neq 0$ increases the values of I_d , but but varying $\ell \neq 0$ does not induce appreciable variations on the intrinsic dimensions. Nevertheless, the integrable point in parameter space is reliably picked out by \bar{I}_d .

VIII. CONCLUSIONS

In this work we have investigated how the complexity of Lindblad dynamics is reflected in the structure of the corresponding quantum trajectories by determining their intrinsic dimension. While the ensemble-averaged Lindblad dynamics rapidly converges to a steady state which does not retain any memory of the spectral structure of the Lindbladian, the trajectories are not stationary and in general occupy lower dimensional subsets of the Hilbert space. The dimensionality of these structures reflects the complexity of the underlying Lindbladian, and shows signatures of properties that impose constraints on the dynamics such as integrability or the decoupling of the BBGKY hierarchy. It is not a priori expected that such constraints have an immediate effect on the dynamics of QT because they are not associated with conservation laws. Our work establishes that these constraints impose correlations between trajectories which have the effect of reducing their complexity.

The integrable points of the dissipative quantum top are characterized by an intrinsic dimension of quantum trajectories equal to one, that increases in presence of perturbations that drive the model towards ergodic dynamics. The dependence of the intrinsic dimension on the model parameters mirrors that of spectral-statistic indicators of quantum chaos, including parameter regimes in which dissipative chaos emerges in the quantum model despite an underlying regular semiclassical limit, highlighting the intrinsically quantum nature of this effect.

For many-body models integrable trajectories remain complex, but are consistently associated to local minima of the intrinsic dimension in the space of model parameters. Adding generic perturbations in an ergodic regime does not significantly change the intrinsic dimension. A qualitatively similar picture is obtained for dissipative models with a decoupling point of their BBGKY hierarchy, where the intrinsic dimension is again observed to exhibit a local minimum, signaling a drop in the complexity of the underlying trajectories.

Altogether, our findings establish the intrinsic dimension as a versatile data-driven probe of complexity in open quantum systems, capable of distinguishing dynamical regimes beyond what is accessible from ensemble-averaged observables alone, while also offering a bridge towards notions of classical chaos.

IX. ACKNOWLEDGEMENTS

This work has been supported by the ERC under grant agreement n.101053159 RAVE (RF, ET), by the PNRR MUR project PE0000023-NQSTI (RF, MC), by the EPSRC under grant EP/X030881/1 (FHLE), and by the PRIN 2022 (2022R35ZBF) - PE2 - “ManyQLowD” (MC). FHLE and RF thank the Institut Henri Poincaré (UAR 839 CNRS-Sorbonne Université) and the LabEx CARMIN (ANR10-LABX-59-01) for their support.

Appendix A: Semiclassical limit and the GHS conjecture

The quantum top is semiclassical when the spin S is large. In particular, it becomes equivalent to a classical continuous angular momentum, defined by the reduced magnetization operators $\hat{m}_\alpha = \hat{S}_\alpha/S$. In this limit the spectrum of each component becomes dense, and the angular momentum algebra turns into $[\hat{m}_\alpha, \hat{m}_\beta] = i\epsilon_{\alpha\beta\gamma}\hat{m}_\gamma/S$, where $1/S$ becomes an effective Planck constant that vanishes for $S \rightarrow \infty$. The Lindblad Eq. (14) implies the adjoint equation

$$\frac{d}{dt}\langle\hat{m}_\alpha\rangle = i\langle[\hat{H}, \hat{m}_\alpha]\rangle + \frac{\gamma}{S}\langle\hat{S}_+\hat{m}_\alpha\hat{S}_- - \frac{1}{2}\{\hat{S}_+, \hat{S}_-\}, \hat{m}_\alpha\rangle.$$

Denoting $m_\alpha \equiv \langle\hat{m}_\alpha\rangle$, it is a matter of algebra to show that the system, up to order $1/S$ corrections that arise from $\langle\hat{m}_\alpha\hat{m}_\beta\rangle = m_\alpha m_\beta + O(1/S)$, is equivalent to

$$\dot{m}_x = \omega_z m_y - 2g m_y m_z + 2\gamma m_x m_z \quad (A1a)$$

$$+ 2k \sum_n \delta(t - n\tau) m_y m_z \quad (A1b)$$

$$\dot{m}_y = \omega_z m_x + 2g m_x m_z - \omega_x m_z + 2\gamma m_y m_z \quad (A1b)$$

$$\dot{m}_z = \omega_x m_y - 2\gamma(m_x^2 + m_y^2) \quad (A1c)$$

$$- 2k \sum_n \delta(t - n\tau) m_x m_y .$$

A direct check shows that these equations always conserve the norm of the classical spin so that the dynamics is constrained on the 2-sphere at a fixed $|\vec{m}|^2 = m_x^2 + m_y^2 + m_z^2$. According to the Poincaré-Bendixson theorem, a classic result in the theory of classical non-linear dynamics, in a two-dimensional autonomous flow chaos is topologically forbidden [66]. The dynamics therefore must be regular when $k = 0$ and the only possible attractors are fixed points and limit cycles. Both are known to exist for $k = 0, \omega_x = 0$, where the presence of periodic orbits is related to a boundary time crystal phase [132]. When kicks are introduced the dynamics becomes explicitly time-dependent and chaotic regions appear, as can be seen in Fig. 11.

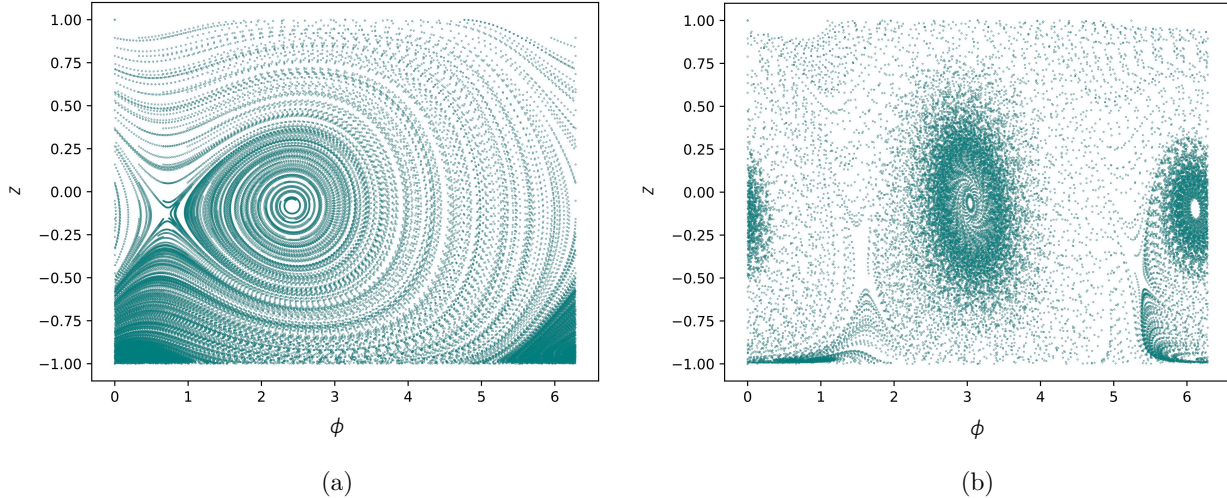


FIG. 11. Phase space orbits of the classical limit of the quantum top in Eq. (A1) for (a) $\omega_x = 3$, $k = 0$; (b) $\omega_x = 2$, $k = 0.2$. The flow is constrained on the sphere with constant $|\mathbf{m}|^2$, and the canonical variables are the standard cylindrical coordinates $z \equiv m_z$, $\cos \phi \equiv m_y/m_x$. The classical dynamics is regular as long as $k = 0$, even when in presence of $\omega_x \neq 0$ as in (a), complying with the Poincaré-Bendixson theorem. Introducing kicks results in the typical chaotic phase space shown in (b).

Appendix B: Intrinsic dimension of individual quantum trajectories

As we noted in Sec. IV C the intrinsic dimension of QT can be calculated in at least two meaningful ways. Throughout the main text of the paper we focused on the intrinsic dimension as a function of time, i.e. the I_d of the set of Hilbert space vectors $|\psi_t\rangle_i$, $i = 1, \dots, N$ reached by evolving N independent QT from an initial state $|\psi_0\rangle$ up to the same time t . Another natural approach would be to focus on individual QT. Here the expectation is that, after an initial transient, QT get confined to a manifold with dimension $I_d < D = \dim_{\mathbb{R}} \mathcal{H}$. As a result the states $\{|\psi_0\rangle, |\psi_i(dt)\rangle, |\psi_i(2dt)\rangle, \dots, |\psi_i(t)\rangle\}$ of the i^{th} QT for sufficiently large t will provide a discrete approximation of the attracting manifold. The time step dt used to simulate a QT is a microscopic quantity, and it can be convenient to subsample the trajectory by considering only the state every $\Delta t = k \cdot dt$ for some integer $k \leq 1$. We calculate the intrinsic dimension of the data set $\mathcal{D}_{i,\Delta t} = \{|\psi_0\rangle, |\psi_i(\Delta t)\rangle, |\psi_i(2\Delta t)\rangle, \dots, |\psi_i(t)\rangle\}$ using the 2-NN method, and the results are then averaged over N trajectories

$$I'_d(\Delta t) = \frac{1}{N} \sum_{i=1}^N I_d^{\text{2-NN}}[\mathcal{D}_{i,\Delta t}]. \quad (\text{B1})$$

In this setting the ratio k between the time step Δt used to construct the data set and the microscopic time step dt of the simulation sets the scale on which the intrinsic dimension is calculated. If Δt is sufficiently small the one-dimensional structure of trajectories is expected to emerge. Here we are interested in what happens when the total evolution time is long enough, so that the trajectory fill a submanifold of the Hilbert space, and Δt is large

enough to lose memory of the microscopic 1d structure.

In panels (a) and (b) of Fig 12 we show the intrinsic dimension along single trajectories for the quantum top as functions of ω_x and k obtained by averaging over $N = 50$ trajectories starting from a fixed random state. Fig 12 (c) and (d) show the analogous results for the dissipative XXZ chain. Using the single-trajectory method we were unable to estimate I_d at the integrable point on the quantum top $\omega_x = 0$, $k = 0$ because the hypothesis of a Pareto distribution for the ratios $\mu_i = r_i^{\text{nnn}}/r_i^{\text{nn}}$ breaks down (cf. Sec. IV B). This is a consequence of the great regularity of long-time integrable trajectories, for which it is not correct to assume that nearest neighbors are extracted from a Poisson process. When a chaotic coupling is switched on, the local structure of the time series changes and we observe the emergence of complex higher-dimensional attractors in the Hilbert space with $1 < I_d \ll D$. Adding even a tiny amount of chaos is sufficient to remove the extreme regularity of the integrable point and it becomes possible to estimate the intrinsic dimension, as is shown in Fig. 13.

This issue does not arise for the dissipative XXZ chains, which instead display a greater sensitivity to the choice of Δt . We observe that small values $\Delta t \sim 10^{-2}$ do not result in a Pareto distribution. For larger values $\Delta t \gtrsim 10^{-1}$ we observe the expected scale dependence of the intrinsic dimension, which arises due to the fact that by decreasing Δt we probe a smaller scale and the values grow, signaling a departure from the microscopic 1d structure. The observed values for the intrinsic dimension and its functional dependencies on ω_x and k for the quantum top, and Δ for the dissipative XXZ chain broadly comparable with the late-time averages \bar{I}_d shown in Figs. 6, 8, confirming that the two methods capture the same submanifold. Small deviations in the estimated

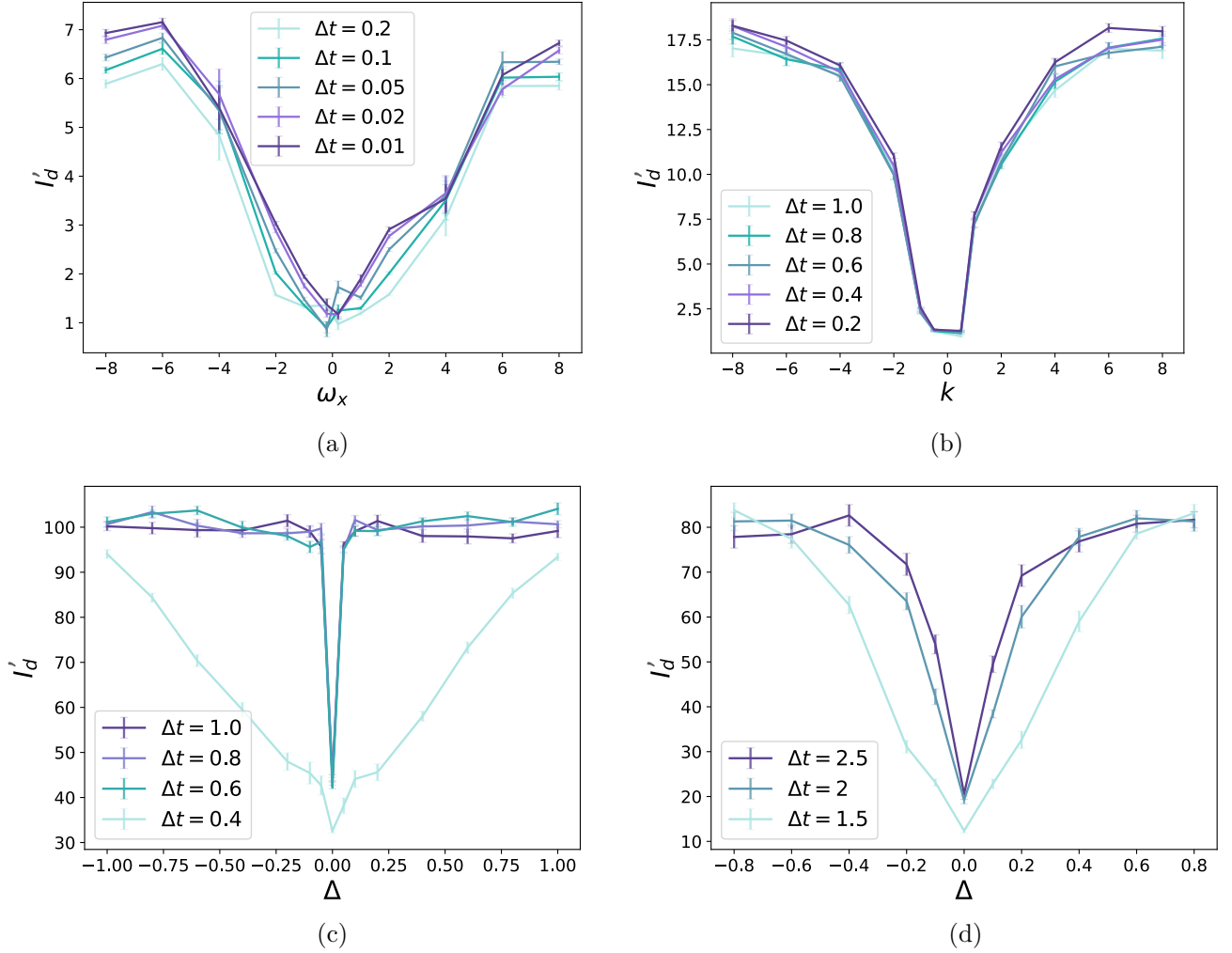


FIG. 12. Intrinsic dimension along individual trajectories. (a) and (b) Dissipative quantum top with $\omega_x = 1$, $g = 5$, $\gamma = 2$ and total spin $S = 30$; (c) Model(A) with $J_1 = 1$, $\gamma_0 = 1$, $J_2 = 0$ and length $L = 8$; (d) Model (B) with $\gamma_1 = 1$. We calculate multiple estimations $I_d^{(i, \Delta t)} = I_d[\mathcal{D}_{i, \Delta t}]$ for each trajectory $i = 1, \dots, N$ using different values of Δt . The errorbars displayed correspond to one standard deviation of the mean of the sample $\{I_d^{(i, \Delta t)}\}_{i=1, \dots, N}$. The mean values of I_d show small variations with Δt , as they tend to increase when the data set is observed at a finer scale able to capture “small” additional dimensions.

values of the intrinsic dimension between the two approaches are to be expected because of the scale dependence, which is difficult to control quantitatively. A more detailed discussion on the scale dependence is included in Appendix C, focusing on the time-averaged intrinsic dimension.

Appendix C: Scale dependence of the intrinsic dimension

The intrinsic dimension of an unknown data manifold one aims to learn depends on the scale at which the manifold is probed, *cf.* our discussion at the end of Section IV B. For a nearest-neighbor based algorithm like the 2-NN method used in this paper, this typically results in a dependence on the number of data points used

to estimate I_d . Under the assumption that additional data points will lie on the same submanifold, generating more samples is expected to probe the data manifold on a finer scale. Focusing on the intrinsic dimension at fixed times and on the data set in Eq. (12), we explore this dependence by increasing the number N of QT used to compute the long-time average \bar{I}_d . To keep track of the scale we compute the typical nearest neighbor distances $\bar{r} = 1/2 \cdot \bar{r}^{nn} + \bar{r}^{nnn}$ in each estimation of $I_d(t)$.

In Fig. 14 we plot the long-time average of \bar{r} , when the QT have settled and $I_d(t)$ has relaxed. This results in a decreasing power-law scaling with N , compatible with the expectation of a fixed submanifold that is being probed at a finer scale. The intrinsic dimension as a function of the scale is shown in Fig 15. At the integrable point of the quantum top $I_d \approx 1$ regardless of the details, whereas chaotic points exhibit an N -dependent I_d , as al-

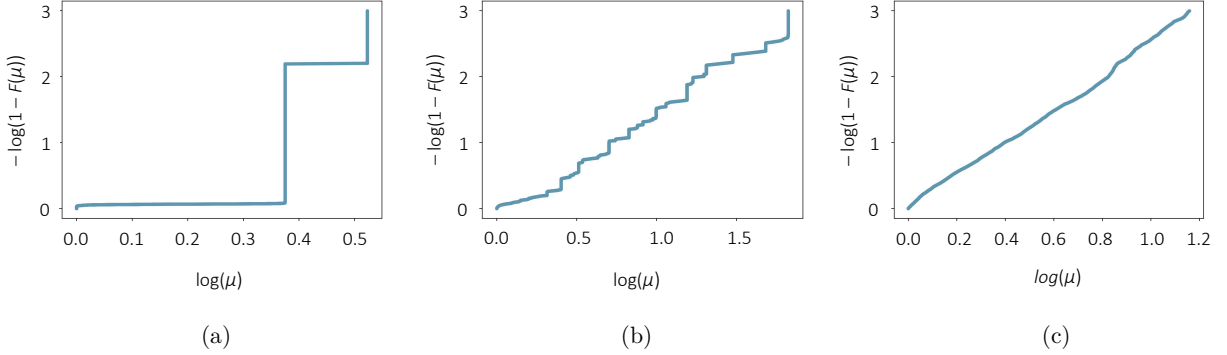


FIG. 13. Empirical cumulative distributions of the nnn/nn ratios for the dissipative quantum top with $\omega_z = 1$, $g = 5$, $k = 0$, starting from (a) with $\omega_x = 0$ to increasingly chaotic models (b) and (c), with $\omega_x = 0.3$ and $\omega_x = 1$. The axis are $\log \mu$, $-\log(1 - \hat{F}(\mu))$ so that for a Pareto distribution the graph is supposed to be linear. The distribution in (a) is very different from the ideal law and I_d cannot be reliably estimated, but increasing ω_x a Pareto law is approached and even when the distribution is not linear yet, like for $\omega_x = 0.3$, an effective I_d can be estimated for most trajectories.

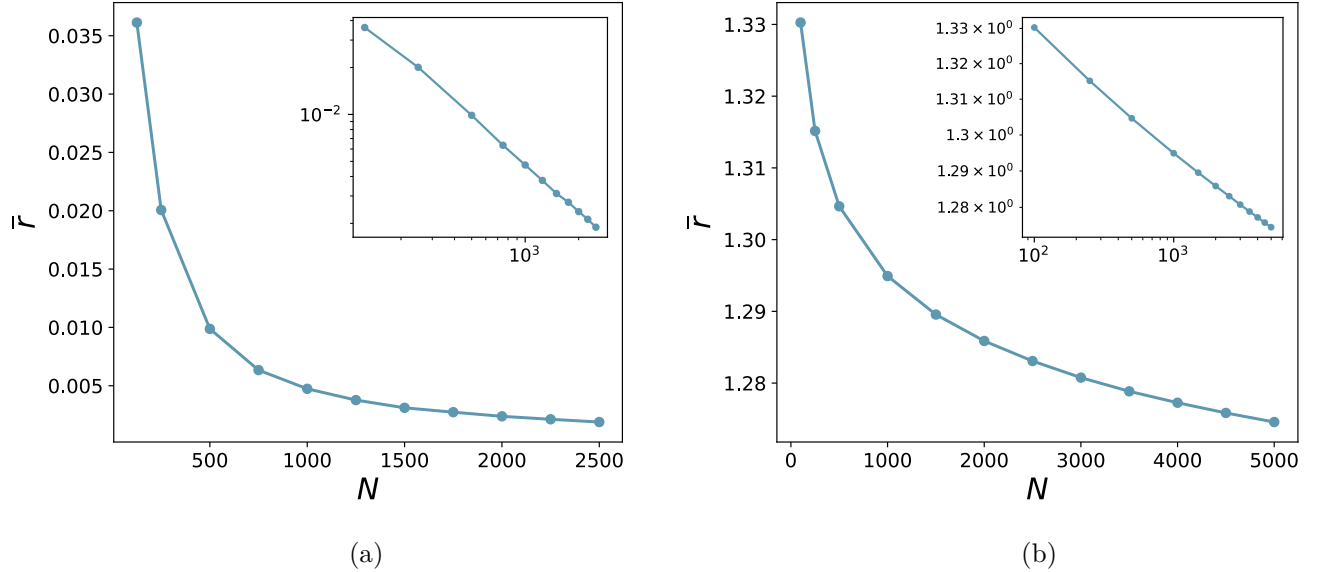


FIG. 14. Typical nearest-neighbor distance \bar{r} as a function of the number of QT: (a) Quantum top with $S = 30$ and $\omega_x = 6.0$; (b) Model (A) with $L = 8$ and $\Delta = 1.0$. The inserts display the same data in log-log scale, highlighting the algebraic decay.

ready noted in Sec. V. The dimensionality increases with the number of QT and displays an approximately linear dependence on the typical nearest-neighbor distances.

The behavior for the dissipative XXZ chain with finite anisotropy is similar, while at the integrable point increasing the number of QT results in a decreasing dimensionality, signaling an emerging simplification of the data structure at a short scale. We note that it would not be appropriate to extrapolate these behaviors to a hypothetical $N \rightarrow \infty$ limit since the intrinsic dimension is expected to eventually display a plateau (up to further deviations induced by noise) [81, 116]. In the range of N considered in our work there was no indication of such a

plateau, and significantly larger numbers of samples may be required to detect one.

A drawback of the approach we have used to analyze the scale dependence of I_d is that the statistical error due to the finite number of samples increases at larger scales, and a more refined analysis could be carried out with other algorithms, such as Gridle [116].

The main conclusion of our analysis of the scale-dependence of the intrinsic dimension is that the reduction in the complexity of QT due to constraints in the underlying Lindblad equation is observed over a very wide range of scales.

[1] G. Vidal, Efficient classical simulation of slightly entangled quantum computations, Phys. Rev. Lett. **91**,

147902 (2003).

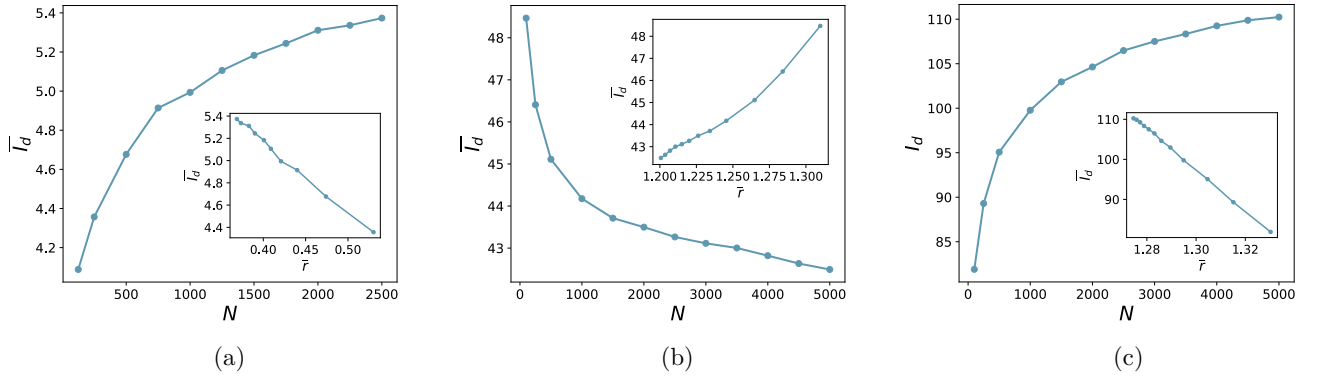


FIG. 15. Scale dependence of the intrinsic dimension, shown as functions of the number of QT and of the typical distances (inserts). (a) Chaotic quantum top with $S = 30$, $\omega_x = 6.0$. (b) XXZ chain subject to dephasing dephasing (Model (A)) with $L = 8$ at its integrable point $\Delta = 0$ and (c) in its ergodic regime at $\Delta = 1$.

- [2] L. Amico, R. Fazio, A. Osterloh, and V. Vedral, Entanglement in many-body systems, *Rev. Mod. Phys.* **80**, 517 (2008).
- [3] V. Veitch, S. A. Hamed Mousavian, D. Gottesman, and J. Emerson, The resource theory of stabilizer quantum computation, *New Journal of Physics* **16**, 013009 (2014).
- [4] M. Howard and E. Campbell, Application of a resource theory for magic states to fault-tolerant quantum computing, *Phys. Rev. Lett.* **118**, 090501 (2017).
- [5] R. Takagi and Q. Zhuang, Convex resource theory of non-gaussianity, *Phys. Rev. A* **97**, 062337 (2018).
- [6] M. Hebenstreit, R. Jozsa, B. Kraus, S. Strelchuk, and M. Yoganathan, All pure fermionic non-gaussian states are magic states for matchgate computations, *Phys. Rev. Lett.* **123**, 080503 (2019).
- [7] B. Dias and R. Koenig, Classical simulation of non-gaussian fermionic circuits, *Quantum* **8**, 1350 (2024).
- [8] D. E. Parker, X. Cao, A. Avdoshkin, T. Scaffidi, and E. Altman, A universal operator growth hypothesis, *Physical Review X* **9**, 10.1103/physrevx.9.041017 (2019).
- [9] M. A. Nielsen, M. R. Dowling, M. Gu, and A. C. Doherty, Quantum computation as geometry, *Science* **311**, 1133–1135 (2006).
- [10] E. Rabinovici, A. Sánchez-Garrido, R. Shir, and J. Sonner, A bulk manifestation of krylov complexity (2023), arXiv:2305.04355 [hep-th].
- [11] E. Rabinovici, A. Sánchez-Garrido, R. Shir, and J. Sonner, Krylov complexity (2025), arXiv:2507.06286 [hep-th].
- [12] L. Susskind, Computational complexity and black hole horizons (2014), arXiv:1402.5674 [hep-th].
- [13] R. A. Jefferson and R. C. Myers, Circuit complexity in quantum field theory, *Journal of High Energy Physics* **2017**, 10.1007/jhep10(2017)107 (2017).
- [14] X. Wang, S. Ghose, B. C. Sanders, and B. Hu, Entanglement as a signature of quantum chaos, *Physical Review E* **70**, 10.1103/physreve.70.016217 (2004).
- [15] L. Vidmar and M. Rigol, Entanglement entropy of eigenstates of quantum chaotic hamiltonians, *Physical Review Letters* **119**, 10.1103/physrevlett.119.220603 (2017).
- [16] A. Nahum, J. Ruhman, S. Vijay, and J. Haah, Quantum entanglement growth under random unitary dynamics, *Phys. Rev. X* **7**, 031016 (2017).
- [17] K. Hashimoto, K. Murata, N. Tanahashi, and R. Watanabe, Krylov complexity and chaos in quantum mechanics, *Journal of High Energy Physics* **2023**, 10.1007/jhep11(2023)040 (2023).
- [18] L. Leone, S. F. E. Oliviero, Y. Zhou, and A. Hamma, Quantum chaos is quantum, *Quantum* **5**, 453 (2021).
- [19] X. Turkeshi, E. Tirrito, and P. Sierant, Magic spreading in random quantum circuits, *Nature Communications* **16**, 10.1038/s41467-025-57704-x (2025).
- [20] P. Sierant, P. Stornati, and X. Turkeshi, Fermionic magic resources of quantum many-body systems (2025), arXiv:2506.00116 [quant-ph].
- [21] A. Paviglianiti, L. Lumia, E. Tirrito, A. Silva, M. Collura, X. Turkeshi, and G. Lami, Emergence of generic entanglement structure in doped matchgate circuits (2025), arXiv:2507.12526 [quant-ph].
- [22] V. E. Korepin, N. Bogoliubov, and A. Izergin, *Quantum inverse scattering method and correlation functions*, Vol. 3 (Cambridge university press, 1997).
- [23] E. Ilievski, M. Medenjak, T. Prosen, and L. Zadnik, Quasilocal charges in integrable lattice systems, *Journal of Statistical Mechanics: Theory and Experiment* **2016**, 064008 (2016).
- [24] R. Nandkishore and D. A. Huse, Many-body localization and thermalization in quantum statistical mechanics, *Annual Review of Condensed Matter Physics* **6**, 15–38 (2015).
- [25] D. Abanin, J. Bardarson, G. De Tomasi, S. Gopalakrishnan, V. Khemani, S. Parameswaran, F. Pollmann, A. Potter, M. Serbyn, and R. Vasseur, Distinguishing localization from chaos: Challenges in finite-size systems, *Annals of Physics* **427**, 168415 (2021).
- [26] C. J. Turner, A. A. Michailidis, D. A. Abanin, M. Serbyn, and Z. Papić, Weak ergodicity breaking from quantum many-body scars, *Nature Physics* **14**, 745–749 (2018).
- [27] M. Serbyn, D. A. Abanin, and Z. Papić, Quantum many-body scars and weak breaking of ergodicity, *Nature Physics* **17**, 675–685 (2021).
- [28] P. Sala, T. Rakovszky, R. Verresen, M. Knap, and F. Pollmann, Ergodicity breaking arising from hilbert space fragmentation in dipole-conserving hamiltonians, *Phys. Rev. X* **10**, 011047 (2020).

[29] S. Moudgalya, B. A. Bernevig, and N. Regnault, Quantum many-body scars and hilbert space fragmentation: a review of exact results, *Reports on Progress in Physics* **85**, 086501 (2022).

[30] M. V. Medvedyeva, F. H. L. Essler, and T. Prosen, Exact bethe ansatz spectrum of a tight-binding chain with dephasing noise, *Physical review letters* **117**, 137202 (2016).

[31] A. A. Ziolkowska and F. H. L. Essler, Yang-baxter integrable lindblad equations, *SciPost Phys.* **8**, 044 (2020).

[32] F. H. L. Essler and L. Piroli, Integrability of one-dimensional lindbladians from operator-space fragmentation, *Physical Review E* **102**, 062210 (2020).

[33] J. Robertson and F. H. L. Essler, Exact solution of a quantum asymmetric exclusion process with particle creation and annihilation, *arXiv preprint arXiv:2105.08828* (2021).

[34] M. de Leeuw, C. Paletta, and B. Pozsgay, Constructing integrable lindblad superoperators, *Physical Review Letters* **126**, 240403 (2021).

[35] D. Paszko, C. J. Turner, D. C. Rose, and A. Pal, Operator-space fragmentation and integrability in pauli-lindblad models (2025), arXiv:2506.16518 [quant-ph].

[36] Y. Li, P. Sala, and F. Pollmann, Hilbert space fragmentation in open quantum systems, *Physical Review Research* **5**, 10.1103/physrevresearch.5.043239 (2023).

[37] A. Marché, G. Moretti, L. Mazza, L. Gotta, and L. Capizzi, Exceptional stationary state in a dephasing many-body open quantum system, *Phys. Rev. Lett.* **135**, 020406 (2025).

[38] D. Wisniacki and G. G. Carlo, Scarring in open quantum systems, *Physical Review E* **77**, 10.1103/physreve.77.045201 (2008).

[39] A. Isar, A. Sandulescu, H. Scutaru, E. Stefanescu, and W. Scheid, Open quantum systems, *International Journal of Modern Physics E* **3**, 635 (1994).

[40] H.-P. Breuer and F. Petruccione, *The Theory of Open Quantum Systems* (Oxford University Press, USA, 2002).

[41] A. Rivas and S. F. Huelga, *Open quantum systems*, Vol. 10 (Springer, 2012).

[42] R. Fazio, J. Keeling, L. Mazza, and M. Schirò, Many-body open quantum systems, *SciPost Phys. Lect. Notes* , 99 (2025).

[43] T. Prosen, Third quantization: a general method to solve master equations for quadratic open fermi systems, *New J. Phys.* **10**, 043026 (2008).

[44] N. Shibata and H. Katsura, Dissipative quantum ising chain as a non-hermitian ashkin-teller model, *Phys. Rev. B* **99**, 224432 (2019).

[45] N. Shibata and H. Katsura, Dissipative spin chain as a non-hermitian kitaev ladder, *Phys. Rev. B* **99**, 174303 (2019).

[46] Y. Li, P. Sala, and F. Pollmann, Hilbert space fragmentation in open quantum systems, *Physical Review Research* **5**, 043239 (2023).

[47] V. Eisler, Crossover between ballistic and diffusive transport: the quantum exclusion process, *Journal of Statistical Mechanics: Theory and Experiment* **2011**, P06007 (2011).

[48] B. Žunković, Closed hierarchy of correlations in markovian open quantum systems, *New Journal of Physics* **16**, 013042 (2014).

[49] S. Caspar, F. Hebenstreit, D. Mesterházy, and U.-J. Wiese, Dissipative bose-einstein condensation in contact with a thermal reservoir, *New Journal of Physics* **18**, 073015 (2016).

[50] D. Mesterházy and F. Hebenstreit, Solvable markovian dynamics of lattice quantum spin models, *Phys. Rev. A* **96**, 010104 (2017).

[51] P. Penc and F. H. L. Essler, Linear response and exact hydrodynamic projections in lindblad equations with decoupled bogoliubov hierarchies (2025), arXiv:2507.13867 [cond-mat.stat-mech].

[52] M. V. Berry, M. Tabor, and J. M. Ziman, Level clustering in the regular spectrum, *Proceedings of the Royal Society of London. A. Mathematical and Physical Sciences* **356**, 375 (1977).

[53] O. Bohigas, M. J. Giannoni, and C. Schmit, Characterization of chaotic quantum spectra and universality of level fluctuation laws, *Phys. Rev. Lett.* **52**, 1 (1984).

[54] R. Grobe, F. Haake, and H.-J. Sommers, Quantum distinction of regular and chaotic dissipative motion, *Phys. Rev. Lett.* **61**, 1899 (1988).

[55] R. Grobe and F. Haake, Universality of cubic-level repulsion for dissipative quantum chaos, *Phys. Rev. Lett.* **62**, 2893 (1989).

[56] F. Ferrari, L. Gravina, D. Eeltink, P. Scarlino, V. Savona, and F. Minganti, Dissipative quantum chaos unveiled by stochastic quantum trajectories, *Phys. Rev. Res.* **7**, 013276 (2025).

[57] D. Villaseñor and P. Barberis-Blostein, Analysis of chaos and regularity in the open dicke model, *Physical Review E* **109**, 10.1103/physreve.109.014206 (2024).

[58] G. Akemann, M. Kieburg, A. Mielke, and T. Prosen, Universal signature from integrability to chaos in dissipative open quantum systems, *Phys. Rev. Lett.* **123**, 254101 (2019).

[59] L. Sá, P. Ribeiro, and T. Prosen, Complex spacing ratios: A signature of dissipative quantum chaos, *Phys. Rev. X* **10**, 021019 (2020).

[60] L. Sá, P. Ribeiro, and T. Prosen, Integrable nonunitary open quantum circuits, *Phys. Rev. B* **103**, 115132 (2021).

[61] R. Grobe and F. Haake, Dissipative death of quantum coherences in a spin system, *Zeitschrift für Physik B Condensed Matter* **68**, 503 (1987).

[62] T. Yoshimura and L. Sá, Robustness of quantum chaos and anomalous relaxation in open quantum circuits, *Nature Communications* **15**, 10.1038/s41467-024-54164-7 (2024).

[63] P. D. Bergamasco, G. G. Carlo, and A. M. F. Rivas, Quantum lyapunov exponent in dissipative systems, *Phys. Rev. E* **108**, 024208 (2023).

[64] A. M. García-García, J. J. M. Verbaarschot, and J.-p. Zheng, Lyapunov exponent as a signature of dissipative many-body quantum chaos, *Phys. Rev. D* **110**, 086010 (2024).

[65] S. H. Strogatz, *Nonlinear Dynamics and Chaos: With Applications to Physics, Biology, Chemistry, and Engineering* (2nd ed.) (CRC Press, 2015).

[66] S. Wiggins, *Introduction to Applied Nonlinear Dynamical Systems and Chaos* (Springer New York, 2003).

[67] C. Gardiner and P. Zoller, *Quantum noise: a handbook of Markovian and non-Markovian quantum stochastic methods with applications to quantum optics* (Springer Berlin, 2004).

[68] H. M. Wiseman and G. J. Milburn, *Quantum Measurement and Control* (Cambridge University Press, 2009).

[69] K. Jacobs, *Quantum Measurement Theory and Its Applications* (Cambridge University Press, 2014).

[70] X. Zheng and C. M. Savage, Quantum trajectories and classical attractors in second-harmonic generation, *Phys. Rev. A* **51**, 792 (1995).

[71] T. Brun, N. Gisin, P. O’Mahony, and M. Rigo, From quantum trajectories to classical orbits, *Physics Letters A* **229**, 267 (1997).

[72] G. Trunk, Statistical estimation of the intrinsic dimensionality of data collections, *Information and Control* **12**, 508 (1968).

[73] L. van der Maaten, E. O. Postma, and J. van den Herik, Dimensionality reduction: A comparative review, *Journal of Machine Learning Research* (2009).

[74] F. Camastra and A. Staiano, Intrinsic dimension estimation: Advances and open problems, *Information Sciences* **328**, 26 (2016).

[75] L. Staiger, Kolmogorov complexity and hausdorff dimension, *Information and Computation* **103**, 159 (1993).

[76] M. Li and P. Vitányi, *An Introduction to Kolmogorov Complexity and Its Applications* (Springer, 2019).

[77] A. A. Brudno, Entropy and the complexity of the trajectories of a dynamic system, *Trudy Moskov. Mat. Obshch.* **44**, 124 (1982).

[78] L. A. L. A. K. Zvonkin, The complexity of finite objects and the development of the concepts of information and randomness by means of the theory of algorithms, *Russian Math. Surveys* **25**, 83 (1970).

[79] F. Camastra and A. Vinciarelli, Intrinsic dimension estimation of data: An approach based on grassberger–procaccia’s algorithm, *Neural Process. Lett.* **14**, 27–34 (2001).

[80] L. Amsaleg, O. Chelly, T. Furion, S. Girard, M. E. Houle, K.-i. Kawarabayashi, and M. Nett, Estimating local intrinsic dimensionality, in *Proceedings of the 21th ACM SIGKDD International Conference on Knowledge Discovery and Data Mining*, KDD ’15 (Association for Computing Machinery, New York, NY, USA, 2015) p. 29–38.

[81] E. Facco, M. d’Errico, A. Rodriguez, and A. Laio, Estimating the intrinsic dimension of datasets by a minimal neighborhood information, *Scientific Reports* **7**, 10.1038/s41598-017-11873-y (2017).

[82] H. Kamkari, B. L. Ross, R. Hosseinzadeh, J. C. Cresswell, and G. Loaiza-Ganem, A geometric view of data complexity: Efficient local intrinsic dimension estimation with diffusion models (2024), arXiv:2406.03537 [cs.LG].

[83] E. Facco, A. Pagnani, E. T. Russo, and A. Laio, The intrinsic dimension of protein sequence evolution, *PLOS Computational Biology* **15**, 10.1371/journal.pcbi.1006767 (2019).

[84] A. Ansuini, A. Laio, J. H. Macke, and D. Zoccolan, Intrinsic dimension of data representations in deep neural networks (2019).

[85] S. Gong, V. N. Boddeti, and A. K. Jain, On the intrinsic dimensionality of image representations, in *Proceedings of the IEEE/CVF Conference on Computer Vision and Pattern Recognition (CVPR)* (2019).

[86] M. Allegra, E. Facco, F. Denti, A. Laio, and A. Mira, Data segmentation based on the local intrinsic dimension, *Scientific Reports* **10**, 10.1038/s41598-020-72222-0 (2020).

[87] P. Pope, C. Zhu, A. Abdelkader, M. Goldblum, and T. Goldstein, The intrinsic dimension of images and its impact on learning (2021), arXiv:2104.08894 [cs.CV].

[88] A. Glielmo, B. E. Husic, A. Rodriguez, C. Clementi, F. Noé, and A. Laio, Unsupervised learning methods for molecular simulation data, *Chemical Reviews* **121**, 9722 (2021).

[89] T. Birdal, A. Lou, L. Guibas, and U. Şimşekli, Intrinsic dimension, persistent homology and generalization in neural networks (2021).

[90] J. Zheng, H. Shen, J. Yang, X. Tang, M. Chen, H. Yu, J. Guo, and X. Wei, Autoencoders with intrinsic dimension constraints for learning low dimensional image representations (2023), arXiv:2304.07686 [cs.CV].

[91] T. Mendes-Santos, X. Turkeshi, M. Dalmonte, and A. Rodriguez, Unsupervised learning universal critical behavior via the intrinsic dimension, *Phys. Rev. X* **11**, 011040 (2021).

[92] T. Mendes-Santos, M. Schmitt, A. Angelone, A. Rodriguez, P. Scholl, H. Williams, D. Barredo, T. Lahey, A. Browaeys, M. Heyl, and M. Dalmonte, Wavefunction network description and kolmogorov complexity of quantum many-body systems, *Physical Review X* **14**, 10.1103/physrevx.14.021029 (2024).

[93] V. Vitale, T. Mendes-Santos, A. Rodriguez, and M. Dalmonte, Topological kolmogorov complexity and the berezinskii-kosterlitz-thouless mechanism (2024), arXiv:2305.05396 [cond-mat.stat-mech].

[94] R. Verdel, V. Vitale, R. K. Panda, E. D. Donkor, A. Rodriguez, S. Lannig, Y. Deller, H. Strobel, M. K. Oberthaler, and M. Dalmonte, Data-driven discovery of statistically relevant information in quantum simulators, *Phys. Rev. B* **109**, 075152 (2024).

[95] H. Cao, D. G. Angelakis, and D. Leykam, Unsupervised learning of quantum many-body scars using intrinsic dimension, *Machine Learning: Science and Technology* **5**, 10.1088/2632-2153/ad4d3f (2024).

[96] C. Sánchez Muñoz, B. Buća, J. Tindall, A. González-Tudela, D. Jaksch, and D. Porras, Symmetries and conservation laws in quantum trajectories: Dissipative freezing, *Phys. Rev. A* **100**, 042113 (2019).

[97] J. Tindall, D. Jaksch, and C. S. Muñoz, On the generality of symmetry breaking and dissipative freezing in quantum trajectories, *SciPost Phys. Core* **6**, 004 (2023), arXiv:2204.06585 [quant-ph].

[98] V. Gorini, A. Kossakowski, and E. C. G. Sudarshan, Completely positive dynamical semigroups of N-level systems, *J. Math. Phys.* **17**, 821 (1976).

[99] G. Lindblad, On the generators of quantum dynamical semigroups, *Comm. Math. Phys.* **48**, 119 (1976).

[100] B. Buća and T. Prosen, A note on symmetry reductions of the lindblad equation: transport in constrained open spin chains, *New Journal of Physics* **14**, 073007 (2012).

[101] V. V. Albert and L. Jiang, Symmetries and conserved quantities in lindblad master equations, *Phys. Rev. A* **89**, 022118 (2014).

[102] F. Haake, *Quantum Signatures of Chaos* (Springer, 2010).

[103] J. P. Garrahan and I. Lesanovsky, Thermodynamics of quantum jump trajectories, *Physical Review Letters* **104**, 10.1103/physrevlett.104.160601 (2010).

[104] F. Carollo, R. L. Jack, and J. P. Garrahan, Un

raveling the large deviation statistics of markovian open quantum systems, *Physical Review Letters* **122**, 10.1103/physrevlett.122.130605 (2019).

[105] G. Perfetto, F. Carollo, and I. Lesanovsky, Thermodynamics of quantum-jump trajectories of open quantum systems subject to stochastic resetting, *SciPost Phys.* **13**, 079 (2022), arXiv:2112.05078 [cond-mat.stat-mech].

[106] S. Pigeon, L. Fusco, A. Xuereb, G. De Chiara, and M. Paternostro, Thermodynamics of trajectories of a quantum harmonic oscillator coupled to n baths, *Phys. Rev. A* **92**, 013844 (2015).

[107] Y. Li, X. Chen, and M. P. A. Fisher, Measurement-driven entanglement transition in hybrid quantum circuits, *Physical Review B* **100**, 10.1103/physrevb.100.134306 (2019).

[108] B. Skinner, J. Ruhman, and A. Nahum, Measurement-induced phase transitions in the dynamics of entanglement, *Phys. Rev. X* **9**, 031009 (2019).

[109] M. J. Gullans and D. A. Huse, Dynamical purification phase transition induced by quantum measurements, *Phys. Rev. X* **10**, 041020 (2020).

[110] P. Grassberger and I. Procaccia, Measuring the strangeness of strange attractor, *Physica D: Nonlinear Phenomena* **9**, 189 (1983).

[111] J. B. Tenenbaum, V. De Silva, and J. C. Langford, A global geometric framework for nonlinear dimensionality reduction, *Science* , 2319 (200).

[112] T. Cox and M. Cox, *Multidimensional Scaling* (Imprint Chapman and Hall/CRC, 2000).

[113] M. Kirby, *Geometric Data Analysis: An Empirical Approach to Dimensionality Reduction and the Study of Patterns* (John Wiley & Sons, Inc., 2000).

[114] I. T. Jolliffe and J. Cadima, Principal component analysis: a review and recent developments, *Philosophical Transactions of the Royal Society A: Mathematical, Physical and Engineering Sciences* **374**, 10.1098/rsta.2015.0202 (2016).

[115] N. Bahadur and R. Paffenroth, Dimension estimation using autoencoders (2019), arXiv:1909.10702 [cs.LG].

[116] F. Denti, D. Doimo, A. Laio, and A. Mira, The generalized ratios intrinsic dimension estimator, *Scientific Reports* **12**, <https://doi.org/10.1038/s41598-022-20991-1> (2022).

[117] S. Recanatesi, S. Bradde, V. Balasubramanian, N. A. Steinmetz, and E. Shea-Brown, A scale-dependent measure of system dimensionality, *Patterns* **3**, <https://doi.org/10.1016/j.patter.2022.100555> (2022).

[118] I. Macocco, A. Mira, and A. Laio, Intrinsic dimension as a multi-scale summary statistics in network modeling, *Scientific Reports* **14**, 10.1038/s41598-024-68113-3 (2024).

[119] F. Haake, M. Kuś, and R. Scharf, Classical and quantum chaos for a kicked top, *Zeitschrift für Physik B Condensed Matter* **65**, 381 (1987).

[120] R. F. Fox and T. C. Elston, Chaos and a quantum-classical correspondence in the kicked top, *Phys. Rev. E* **50**, 2553 (1994).

[121] P. Jacquod, P. Silvestrov, and C. Beenakker, Golden rule decay versus lyapunov decay of the quantum loschmidt echo, *Phys. Rev. E* **64**, 055203 (2001).

[122] J. N. Bandyopadhyay and A. Lakshminarayanan, Entanglement production in coupled chaotic systems: Case of the kicked tops, *Phys. Rev. E* **69**, 016201 (2004).

[123] S. Chaudhury, A. Smith, B. E. Anderson, S. Ghose, and P. S. Jessen, Quantum signatures of chaos in a kicked top, *Nature* **461**, 768 (2009).

[124] C. Neill, P. Roushan, M. Fang, Y. Chen, M. Kolodrubetz, Z. Chen, A. Megrant, R. Barends, B. Campbell, B. Chiaro, A. Dunsworth, E. Jeffrey, J. Kelly, J. Mutus, P. J. J. O’Malley, C. Quintana, D. Sank, A. Vainsencher, J. Wenner, T. C. White, A. Polkovnikov, and J. M. Martinis, Ergodic dynamics and thermalization in an isolated quantum system, *Nature Physics* **12**, 1037–1041 (2016).

[125] U. T. Bhosale and M. S. Santhanam, Periodicity of quantum correlations in the quantum kicked top, *Physical Review E* **98**, 10.1103/physreve.98.052228 (2018).

[126] L. M. Sieberer, T. Olsacher, A. Elben, M. Heyl, P. Hauke, F. Haake, and P. Zoller, Digital quantum simulation, trotter errors, and quantum chaos of the kicked top, *npj Quantum Information* **5**, 10.1038/s41534-019-0192-5 (2019).

[127] E. Vallini and S. Pappalardi, Long-time freeness in the kicked top (2024), arXiv:2411.12050 [cond-mat.stat-mech].

[128] N. Defenu, T. Donner, T. Macrì, G. Paganò, S. Ruffo, and A. Trombettoni, Long-range interacting quantum systems, *Rev. Mod. Phys.* **95**, 035002 (2023).

[129] P. Ribeiro and T. Prosen, Integrable quantum dynamics of open collective spin models, *Physical Review Letters* **122**, 10.1103/physrevlett.122.010401 (2019).

[130] D. Bernard and T. Jin, Open Quantum Symmetric Simple Exclusion Process, *Phys. Rev. Lett.* **123**, 080601 (2019).

[131] G. Barraquand and D. Bernard, Introduction to quantum exclusion processes, arXiv preprint arXiv:2507.01570 (2025).

[132] F. Iemini, A. Russomanno, J. Keeling, M. Schirò, M. Dalmonte, and R. Fazio, Boundary time crystals, *Phys. Rev. Lett.* **121**, 035301 (2018).